Spatial Modeling of Fire in Shrublands using HFire: Model Description and Event Simulation

Suggested Running Head: HFire: Model Description and Event Simulation

Seth H. Peterson[1,*], Marco E. Morais[2], Jean M. Carlson[3], Philip E. Dennison[4], Dar A. Roberts[5], Max A. Moritz[6] and David R. Weise[7]

[1]Department of Geography, University of California, Santa Barbara, CA 93106, USA. telephone: 805 893 4434; email: seth@geog.ucsb.edu
*corresponding author

[2]The Aerospace Corporation, 2350 E. El Segundo Blvd, El Segundo, CA 90245, USA; telephone: 805 558 7722; email: marcoemorais@yahoo.com

[3]Department of Physics, University of California, Santa Barbara, CA 93106, USA. telephone: 805 893 8345; email: carlson@physics.ucsb.edu

[4]Center for Natural and Technological Hazards and Department of Geography, University of Utah, Salt Lake City, UT 84112, USA
telephone: 801 581 8218; email: dennison@geog.utah.edu

[5]Department of Geography, University of California, Santa Barbara, CA 93106, USA. telephone: 805 893 2276; email: dar@geog.ucsb.edu

[6]Center for Fire Research and Outreach, Department of Environmental Science, Policy, & Management, University of California, Berkeley, CA 94720, USA
email: mmoritz@nature.berkeley.edu

[7]Forest Service, Pacific Southwest Research Station, Forest Fire Laboratory, 4955 Canyon Crest Drive Riverside, California 92507, USA. email: dweise@fs.fed.us

Keywords: fire spread model; raster; Rothermel; wildfire; Southern California; chaparral

Abstract

A raster based, spatially explicit model of surface fire spread called HFire is introduced. HFire uses the Rothermel fire spread equation to determine one dimensional fire spread, which is then fit to two dimensions using the solution to the fire containment problem and the empirical double ellipse formulation of Anderson. HFire borrows the idea of an adaptive time step from previous cell contact raster models and permits fire to spread into a cell from all neighboring cells over multiple time steps as is done in the heat accumulation approach. The model has been developed to support simulations of single fire events and long term fire regimes. The model implements equations for surface fire spread and is appropriate for use in grass or shrubland functional types. Model performance on a synthetic landscape, under controlled conditions was benchmarked using a standard set of tests developed initially to evaluate FARSITE. Additionally, simulations of two Southern California fires spreading through heterogeneous fuels, under realistic conditions showed similar performance between HFire and FARSITE, good agreement to historical reference data, and shorter model run times for HFire. HFire is available for download: http://firecenter.berkeley.edu/hfire.

Fifty-Word Summary

An efficient raster fire spread model named HFire is introduced. HFire can simulate single fire events or long term fire regimes, using the same fire spread algorithm. This paper describes the HFire algorithm, benchmarks the model using a standard set of tests developed by Finney (1998) for FARSITE, and compares historical and predicted fire spread perimeters for two Southern California fires.

1. Introduction

Interest in predictive models of wildland fire spread has existed more or less continuously since the late 1930s and has produced a substantial body of published information (Fons 1946; Catchpole and DeMestre 1986; Weber 1991; Pitts 1991). From the perspective of a fire manager working for a land management agency in the United States, the culmination of this accumulated knowledge is encapsulated in the United States (US) fire prediction system. The fire spread predictions used by the current system are based upon a semi-empirical formulation first presented by Rothermel in 1972. This system has been implemented operationally in the form of programmable hand held calculators in the late 1970s (Rothermel 1983), the BEHAVE minicomputer program in the middle 1980s (Andrews 1986), and the FARSITE fire spread model in the middle 1990s (Finney 1998). FARSITE is unique because it is the first component of the national system which provides spatially explicit predictions of fire spread. In addition to the use of the Rothermel equation for modeling surface fire spread, FARSITE adds crown fire and spot fire modules for use during extreme wildfire conditions.

HFire (Highly Optimized Tolerance Fire Spread Model) is a spatially explicit model of surface fire spread through shrubland fuels for real time use during complex fire situations. HFire and FARSITE are based on the Rothermel equation, but HFire uses a more computationally efficient raster based algorithm to model fire spread in two dimensions. This allows for both near real time fire behavior prediction and multi-century fire regime modeling.

This paper introduces and describes the HFire fire spread algorithm, benchmarks the model using a standard set of tests developed by Finney (1998) for FARSITE, and compares historical and predicted fire spread perimeters for two Southern California fires.

2. Rothermel rate of spread model

Fire spread models can be classified according to the degree to which they are based on empirical data or physical principles (Weber 1991). Fully empirical models do not attempt to simulate the physical phenomena and instead rely on statistical correlation between variables known to influence fire spread (e.g. wind speed or slope). A very simple empirical model of fire spread might be

$$R = aU^{b}, \quad (1)$$

where the rate of fire spread, R (m s^{-1}), is the product of the windspeed, U (m s^{-1}), raised to an empirically determined power, b (unitless), and an empirically determined constant, a (unitless). Nelson and Adkins (1988) used dimensional analysis to construct a similar model from data collected during laboratory and field experiment wind driven fires. A weakness of any fully empirical model is that predictions made for fire spread under conditions that were not explicitly tested for may be unreliable.

Fully physical models differentiate among the different modes of heat transfer from burning to unburned fuel and link to the meteorological equations of motion in a way that captures the feedback between the fire and local weather conditions (Linn 1997; Linn *et al.* 2002). These types of models offer high fidelity, but are computationally intense and thus not suitable for use in a real time operational setting or for multi-year simulations of fire regime (Hanson *et al.* 2000).

Semi-empirical/semi-physical models are a blend of the two approaches. In a fully physical model, a heat transfer calculation is used to estimate the rate of fire spread from the ratio of flux between burning and unburned fuel,

$$R = \frac{\sum_{m=1}^{u} q_m}{\sum_{n=1}^{v} Q_n}, \qquad (2)$$

where R is equal to the ratio of the heat received by unignited fuel ahead of the fire, q (J s^{-1} m^{-2}), over the heat required to ignite the fuel at the leading edge of the fire, Q (J m^{-3}) (Williams 1976). Semi-physical models make some simplifications in how each of the u and v components in the heat transfer equation (2) are described. The Rothermel equation (1972) resembles the heat transfer equation, but substitutes the flux components with representative empirically derived terms,

$$R = \frac{I_R\ \xi\ (1 + \Phi_w + \Phi_s)}{\rho_f \varepsilon\ Q_{ig}}, \qquad (3)$$

where I_R is the reaction intensity (J s^{-1} m^{-2}), ξ is the propagating flux ratio, Φ_w is the wind factor, Φ_s is the slope factor, ρ_f is the fuel bed bulk density (kg m^{-3}), ε is the effective heating number, and Q_{ig} is the heat of preignition (J kg^{-1}). The Rothermel equation computes the steady-state rate of fire spread in the direction of maximum fire spread and assuming wind and slope are aligned in this direction. As a result, some other models must be used to compute the rate of fire spread in other directions and when wind and slope are not aligned with the direction of maximum spread.

3. Two dimensional fire spread modeling approaches

Both vector and raster based approaches have been used to model fire spread in two dimensions. The vector based approach simulates fire spread as a continually expanding fire polygon (Anderson *et al.* 1982) and is the basis for the FARSITE model. Raster schemes of representing two dimensional fire growth partition the modeling domain into regularly spaced square or hexagonal lattices that restrict the direction of fire spread to the cardinal axes associated with an individual cell (Kourtz and O'Regan 1971; Frandsen and Andrews 1979; Green *et al.* 1990; Clarke *et al.* 1994; Hargrove *et al.* 2000; Berjak and Hearne 2002). In these models, the simulated fire typically spreads from cell to cell through the simulation domain using cell contact or heat accumulation.

In the vector approach to modeling fire spread, the fire perimeter at any point in time is represented by an infinitely thin arc consisting of a set of n coordinate pairs, known as vertices, in a Cartesian plane. Empirical relationships developed by Anderson (1983) are used to predict the dimensions of a fire spreading as an ellipse from the maximum rate of fire spread and the local wind and slope conditions. The envelope formed by the line tangent to the n fire prediction ellipses defines the leading edge of the fire. The number of coordinate pairs, n, relative to the length of the perimeter, l, dictates the spatial resolution of the predicted fire spread; referred to as “perimeter resolution” in FARSITE. One of the weaknesses of the vector approach is the difficulty in choosing an appropriate perimeter resolution. Clarke *et al.* (1994) observed from historical fire scars that fire perimeter length is strongly dependent upon scale and this suggests a uniform perimeter resolution may not be appropriate. Another weakness of the vector approach is the need for a computationally expensive fire spread perimeter discretization procedure (Richards, 1990) at the end of each time step in order to resolve fire crossovers and unburned islands. In a critical evaluation of a fire spread model implementing Huygens' Principle, French *et al.* (1990) found that the model performance suffered under increasingly heterogeneous conditions.

The cell contact based approach to fire spread, first presented by Kourtz and O'Regan (1971), is consistent with an interpretation of fire spread as a series of discontinuous ignitions spanning the length of an individual cell. The strength of this approach is that it is extremely computationally efficient because the simulation clock increments in nonuniform intervals based on the amount of time required to spread into an adjacent cell; this is sometimes referred to as the time-of-arrival (TOA) of the fire perimeter. This eliminates the redundant computations that are made when operating with a uniform time step. The weakness of the contact approach is that events are generated based only upon the influence of the single fastest spreading neighbor, and fire spread into a cell that is the cumulative effect of multiple neighboring cells or prior heating is neglected (Green 1983). French *et al.* (1990) critically evaluated the performance of several contact based raster models (Kourtz and O'Regan 1971; Frandsen and Andrews 1979) and found that the fire shapes produced were severely distorted. These results arose even in cases where the choice of the underlying lattice was varied from a square network of cells to a hexagonal network, effectively increasing the degrees of freedom of the fire spread.

The heat accumulation approach to raster fire spread mitigates the fundamental weakness of the contact based approach by enabling the rate of spread of fire into a cell to be the sum of the contribution of neighboring ignited cells during prior time steps (Green 1983; Green *et al.* 1990). The heat accumulation model iterates over fixed time intervals, known as the time step, visiting every cell in the simulation domain and tabulating the quantity of heat received by that cell from all of its neighbors. After receiving some threshold quantity of heat, a cell is considered ignited and begins delivering heat to neighboring cells. Although the phrase “heat accumulation” suggests that there is a physical basis for the method used to describe the ability of a cell to absorb and emit heat, all implementations to date have used fully empirical or semi-empirical/semi-physical models of fire spread as surrogates for the physical properties and mechanisms of fire spread (Green 1990). French *et al.* (1990) also empirically evaluated the performance of a heat accumulation model (Green 1983) and found that it was more computationally intensive than the contact based approach because of the relatively small elapsed time step required to capture rapid fire spread. However, the added cost appeared worthwhile because the fire spread perimeters produced from the heat accumulation model were less distorted in comparison to the contact based models.

4. The HFire model

4.1 Model description

HFire (Morais 2001) is raster model of surface fire spread based on the Rothermel (1972) fire spread equation and the empirical double ellipse formulation of Anderson (1983). A state machine is used to track the movement of the fire through the cells in the simulation domain. The model is efficient and can be used to simulate single fire events or fire regimes that develop over hundreds of years. Single event simulations driven by historical or predicted data are completely deterministic. Although not discussed in this paper, the model can be used for multi-year simulations of fire regime (many hundreds of years) featuring stochastic historical weather patterns, ignition frequency and location, simulated Santa Ana events, and dynamic fuels regrowth (Moritz *et al.* 2005). Other uses for Hfire include examining sensitivity to weather inputs (Clark *et al.* in press) and effectiveness of fire suppression (Ntaimo *et al.* 2004).

4.2 Model inputs

HFire model inputs can be subdivided into three groups: (1) fuel variables; (2) terrain variables; and (3) environmental variables (Table 1).

#Insert Table 1 Approximately Here#

4.2.1 Fuel variables

Fuels are described using the parameter sets (fuel models) for the Rothermel model developed by Albini (1976). The 13 Northern Forest Fire Laboratory (NFFL) standard fuel models (Albini 1976) or user defined custom fuel models (Burgan and Rothermel 1984) are supplied via a look-up table that is used to map the fuel model number of a pixel to a parameter set. Since the Rothermel equation assumes a homogeneous fuel bed, a method of averaging the collections of fuel particles used by the fuel modeling system is required. HFire uses the surface-area-to-volume weighting scheme described by Rothermel (1972) to synthesize the fuel particle attributes into single characteristic value of the fuel bed. Although some fuel variables such as fuel load and depth vary annually due to disturbance and seral stage, the change in these properties within a single year is small enough to justify holding them constant during a year of simulation time. Fuel moisture varies on a daily basis (dead) or seasonal basis (live) and is treated as an environmental variable by the model.

4.2.2 Terrain variables

The terrain variables used by the model (elevation, slope and aspect) are typically computed from a digital elevation model (DEM) using a geographic information system (GIS). These are held constant for the duration of single event and multi-year simulations.

4.2.3 Environmental variables

The environmental variables used by the model can vary in both time and space. Time varying environmental inputs can be specified to a minimum resolution of one hour[1]. This constraint does not reflect a limitation of the internal simulation clock, but is imposed because estimates for these parameters are commonly taken from Remote

[1] This restriction will be relaxed in future versions of HFire to allow time tagged inputs specified at any resolution.

Automated Weather Stations (RAWS) that report data in one hour intervals. Spatially varying environmental inputs can be specified at a different spatial resolution from the terrain and fuels variables and up to a minimum temporal resolution of one hour. Diagnostic wind models are a potential source for spatially varying weather inputs (Butler *et al.* 2006) and remote sensing is a potential source for live fuel moisture (Dennison *et al.* 2003; Dennison *et al.* 2005; Roberts *et al.* 2006).

HFire assumes wind speed and direction data are measured at the conventional reference height for RAWS stations in the United States, 6.1 meters above the top of the fuel bed. HFire uses an approximation[2] to the logarithmic reduction formula given by Albini and Baughman (1979) to compute the wind speed experienced at mid-flame from the wind speed measured at the reference height,

$$U_{mid} = \frac{U_{ref}}{\ln\left[\frac{h_{ref} + (0.36 h_{mid})}{0.13 h_{mid}}\right]} \quad , \tag{4}$$

where U_{mid} is the mid-flame wind speed (m s^{-1}), U_{ref} is the wind speed measured at the reference height (m s^{-1}), h_{ref} is the reference height (m), and h_{mid} is the mid-flame height (m). In HFire the mid-flame height, h_{mid}, is assumed to be equal to twice the fuel bed depth. Although others have suggested that a logarithmic wind speed reduction profile may be less accurate during periods of local atmospheric instability (Beer 1990) and

[2] There is a slight discrepancy between the mid-flame wind speed computed from Albini and Baughman (1979) and the mid-flame wind speed computed using BEHAVEPlus. The wind speed adjustment factor (WAF) used in BEHAVEPlus (WAF_{BHP}) can be recovered from the Albini and Baughman equation (WAF_{AB79}) using the following linear equation: $WAF_{BHP} = WAF_{AB79} * 1.371817779 + 0.046171831$. The results reported in this paper use the WAF from BEHAVEPlus.

during nighttime conditions (Rothermel *et al.* 1986), HFire utilizes this adjustment throughout the duration of the simulation.

4.3 Two dimensional fire spread

There is widespread agreement that fire spread under steady homogeneous conditions and in the presence of wind and topography roughly approximates an expanding ellipse. Anderson (1983) describes fire spread as a double ellipse, where the length to width ratio is a function of the mid-flame wind speed. A double ellipse allows for different equations to describe the forward and backward spreading ellipses.

Since Rothermel's original fire spread equation assumes that the wind is aligned directly with slope, the effect of cross-slope winds must be taken into account. HFire uses the technique defined in Rothermel (1983) [Figure IV-8] to compute the cross-slope rate of spread vector by adding two rate of spread vectors, one computed using the observed winds without slope and another using the slope and no wind. The wind speed in the direction of the cross-slope rate of spread vector, termed the effective wind speed, U_{eff} (m s^{-1}), is used to compute the length to width ratio of an ellipse Rothermel (1991) [Eqn 9],

$$\frac{L}{W} = 1 + 0.5592\, k\, U_{eff}\,, \qquad (5)$$

where L is equal to the length (m) and W is equal to the width (m) of the predicted elliptical dimensions. The coefficient k is an addition to Rothermel's (1991) equation[3] that

[3] Eqn (9) in Rothermel (1991) is a linearization of an exponential function suggested by Andrews (1983) where U is given in mi hr^{-1}. Eqn (5) in this paper uses U in m s^{-1} and as a result the coefficient 0.25 in mi hr^{-1} has been divided by (1609.344 m/ 3600s) in order for L and W to remain unitless.

we have included in HFire and termed the ellipse adjustment factor (EAF). The EAF is included in HFire as a correction factor for grid induced effects associated with the raster based algorithm. The raster based algorithm generally produces narrower, more angular fire shapes than FARSITE when $k = 1.0$ (i.e. no EAF correction), values of k less than 1.0 widen the fire front for HFire. The rationale for the EAF is explained in more detail following Eqn (7).

Albini and Chase (1980) provide a formula [Eqn 8] for determining the eccentricity of an ellipse, E, such that $0 < E < 1$ and using the length, L, and width, W:

$$E = \frac{\sqrt{(\frac{L}{W})^2 - 1}}{(\frac{L}{W})} . \qquad (6)$$

Given the predicted eccentricity, E, of the fire calculated from the effective wind speed and the rate of maximum fire spread calculated from the Rothermel equation, R_{max}, the solution to the fire containment problem (Albini and Chase, 1980) provides the rate of fire spread at arbitrary angles from the maximum:

$$R_\theta = R_{\max} \frac{(1 - \mathrm{E})}{(1 - \mathrm{E} \cos\theta)} , \qquad (7)$$

where R_θ, is the rate of fire spread (m s^{-1}), at some angle θ (degrees), from the direction of the maximum rate of fire spread. The derivative of Eqn 7 with respect to the angle, θ, is largest at small angles, $0° < \theta < +/- 45°$. For example, the eccentricity for typical length to width ratios (12:1 to 3:1) is on the order of 0.9 and for this value, R_{45} is reduced to 27% of R_0 using Eqn 7. Hence, for a raster model allowing fire spread to eight neighbors, where the values of the angle θ in Eqn 7 are restricted to multiples of 45° in the range [-180°, 180°], the region from 0^o to +/- 45^o is undersampled and poorly approximates the true shape of the function. As a result, the shape of the heading portion of the fire is angular rather than rounded, in comparison to a vector model.

The EAF is introduced to compensate for this distortion. The effect of the EAF on predicted fire shapes on a landscape with flat terrain, homogeneous fuels, and under uniform wind conditions is shown in Figure 1 (Section 5.1.2). In all cases the distance spread in the direction of the maximum rate of fire spread (from the ignition point to the fire front) is unchanged, but the fire front is less pointed (EAF < 1.0) than the raster realization of Anderson's (1983) standard fire spread ellipse (EAF = 1.0). For example, for an effective wind speed of 5 m s^{-1}, R_{45} is reduced to 25% of R_0 with EAF = 0.5 and to 11% with EAF = 1.0. In cases where conditions are homogeneous, setting the EAF < 1.0 reduces the sharpness along the heading portion of the fire. In cases where conditions are heterogeneous, the heading portion of the fire will become more blunted as the direction of the maximum rate of fire spread changes, and an EAF closer to 1.0 can be used. Recommendations for setting the EAF appropriately are made in Section 5.

In any three-by-three neighborhood of cells, a fire located at the center of the neighborhood has the potential of spreading to all eight adjacent neighbors. The fire spread distance in the direction of a neighboring cell located at some angle θ, in degrees, from the cell center during the n^{th} iteration $d_{\theta,n}$ is equal to the rate of fire spread in the direction of the neighbor during the n^{th} iteration $R_{\theta,n}$ multiplied by the duration of the time step t_n:

$$d_{\theta,n} = R_{\theta,n}\ t_n \,. \qquad (8)$$

Under homogeneous conditions an eight sided figure will always emerge because the underlying raster provides eight degrees of freedom.

4.4 Adaptive time step

The cell size, Δd, provides a lower limit on the distance between adjacent cells in the simulation. The terrain distance, d_{xyz}, is necessary for tracking fire spread parallel to the ground and is computed from a pair of cells in three dimensional Cartesian space $\{x_1, y_1, z_1\}$ and $\{x_2, y_2, z_2\}$ as:

$$d_{xyz} = \sqrt{(x_1 - x_2)^2 + (y_1 - y_2)^2 + (z_1 - z_2)^2} \;. \qquad (9)$$

The terrain distance between adjacent cells at the same elevation and connected via one of the four cardinal directions, 0 (north), 90 (east), 180 (south), or 270 (west) degrees, will always be equal to or longer than the cell size. Similarly, the terrain distance between cell centers connected by a diagonal will always be longer than the cell size. Thus, the cell size, Δd, divided by the maximum rate of fire spread at all cells in the simulation domain during the n^{th} iteration, max $|R_{max,n,}|$, yields the minimum amount of time, in seconds, that can occur in the simulation before the fire may have traveled from one cell center to another during a single time step. This provides the basis[4] for the size of the time step used during the n^{th} iteration, t_n:

[4] The distance past a neighboring cell center that a fire spreads during a single iteration is termed the "slop over". HFire properly handles "slop over", but an attempt is made to minimize the frequency with which it occurs by scaling the time step computed using Eqn (10) by 0.25. More details are provided in section 4.5.

$$t_n = \frac{\Delta d}{\max |R_{\max,n}|} \quad . \tag{10}$$

Since the size of the time step will vary with fire behavior, incrementing more slowly when fire spread is rapid and vice-versa, this is referred to as an adaptive time step.

4.5 Modeling fire spread at sub-cell resolutions

Given a method for computing the rate of fire spread in any direction and for determining an appropriate time step from the fastest spreading component of the fire, a state machine is used to track the movement of the fire through the cells in the simulation domain. At any instant in the simulation, all cells in the simulation domain are assigned one of four possible states.

1. Cell is **unburnable** [U].
2. Cell is flammable, but **not currently ignited** [N].
3. Cell is flammable and is **ignited**, but fuel is not yet consumed [I].
4. All fuel in cell has been **consumed** by the fire [C].

At the start of the simulation, all cells are in the unburnable [U] or not currently ignited [N] states. Unburnable cells [U] correspond to areas without the potential to burn, such as rock outcrops, and water bodies, including the ocean, lakes, and perennial streams. There are no transitions to or from the unburnable state to any of the other three states.

During the simulation there are two possible events that can result in the transition of a cell from the not currently ignited state [N] to the ignited state [I]. The first type of transition event is an independent ignition that represents a new fire. Independent ignitions can be specified by the user in two ways. For single event simulations, the user typically supplies a file containing the coordinates of cells that will be ignited [I] at the start of the first iteration in the simulation. For multi-year simulations, the user specifies two types of ignition probabilities: an overall temporal frequency for ignitions and a surface containing the relative probability of ignition for each cell. Ignitions occur stochastically in time and space.

The second type of transition event occurs when a fire spreads into the cell from an adjacent cell. HFire implements fire spread as follows. The simulation maintains a list of all cells that are in the ignited state [I]. Two arrays are associated with each element of this list. The first array is used to accumulate the distance over multiple time steps that the fire has traveled in each of the eight possible directions. The second array is used to store the terrain distance, d_{xyz}, between adjacent cells in each direction. When the accumulated distance in a direction exceeds the terrain distance in that direction, then the adjacent cell in that direction is transitioned from the not ignited state [N] to the ignited state [I]. Any excess distance, termed "slop over", is applied to the array of accumulated distances for the newly ignited cell in the direction of fire spread.

During the simulation there are two possible events that can result in the transition of a cell from the ignited state [I] to the consumed state [C]. The first type of transition event is triggered when the eight neighbors of a cell are in the ignited state [I] or unburnable state [U]. Cells in this configuration are typically located in the interior portions of an expanding fire. This is not meant to imply that cells in the consumed state [C] are not undergoing postfrontal combustion, only that the energy released from these cells no longer contributes to the forward rate of spread of the fire. The second type of transition event occurs when a fire is extinguished, this is important for the multi-year model runs.

Fire does not burn in a cell indefinitely. Fire extinction refers to the transition of a cell from the ignited state [I] to the not ignited state [N] or from the ignited state [I] to the consumed state [C]. The Rothermel model given in Eqn (3) does not describe the conditions under which a fire is extinguished. As a result, the simulation uses a few additional heuristics to trigger extinction. First, a cell in the ignited state [I] that has burned longer than a user specified threshold without propagating to all adjacent burnable neighbors will trigger an extinction transition, this is implemented in the simulation by tracking the time since each cell was ignited. Second, a cell in the ignited state [I] with a maximum rate of fire spread that falls below a user specified threshold will trigger an extinction transition. In both cases, the user controls whether all extinction transitions will go from ignited [I] to not ignited [N] or from ignited [I] to consumed [C].

5. Simulations and results

In this Section we describe the results of a series of numerical simulations which aim to evaluate the performance of HFire. This consists of two separate series of tests. The first set of tests consists of a series of benchmarks on synthetic, homogeneous landscapes under simplified burning conditions. Our study deliberately follows the initial landmark validation of the FARSITE implementation of the Rothermel equations, as designed by

Finney (1998). For all of the HFire simulations we run comparison simulations with FARSITE, using the same inputs, enabling a direct comparison of the results.

The second set of tests involves simulations of two historical fires with mapped topography and vegetation and measured weather. There are no obvious raster based artifacts in the HFire perimeter shapes -- for real landscapes, variations in topography, vegetation, and weather appear to be more important factors in determining fire shape than the underlying algorithm. Results for a third fire are presented as supplemental online material.

All tests are performed with the same inputs, with the exception of dead fuel moisture. HFire utilizes hourly 10 hour dead fuel moisture data from RAWS stations and the 1 hour and 100 hour dead fuel moistures are determined from the 10 hour values +/- a user defined constant. For FARSITE 1, 10, and 100 hour dead fuel moistures are initialized at the beginning of the simulation period and are modified using a sinusoidal function whose shape is dictated by air temperature and humidity.

FARSITE contains modules for predicting fire spread in grassland, shrubland, and forested landscapes, whereas HFire is designed for chaparral landscapes comprised of grasslands and shrublands only. FARSITE modules for forested landscapes which allow for spotting and crown fires are not applicable. In addition, the FARSITE fire acceleration module is disabled so that a straight comparison between the two model implementations of the Rothermel equations could be performed.

Agreement between HFire and FARSITE modeled fire perimeters, as well as between modeled and historic fire perimeters, are assessed using the Sørensen metric. The

Sørensen metric (Greig-Smith 1983; Perry *et al.* 1999) measures agreement between two areas:

$$S = \frac{2a}{(2a + b + c)}, \quad (11)$$

where a is the intersection of the area burned in the two models, b is the area burned by model A but not model B, and c the area burned by model B but not model A. A value of S=1.0 indicates perfect agreement. All calculations are performed on cumulative areas for an individual fire. Perry *et al.* (1999) used the Sørensen metric to assess the accuracy of a simulation of the 1995 Cass Fire in New Zealand.

5.1 Synthetic landscape tests

A series of simple, controlled tests were designed by Finney (1998) to illustrate the response of the FARSITE fire spread model to the primary factors affecting fire spread. These factors include wind speed, wind direction, slope, fuel type, and fuel transitions. They are varied individually and in pairs under otherwise uniform conditions to illustrate model behavior under idealized, controlled conditions. To evaluate HFire we replicated the burning conditions used by Finney (1998) to test the FARSITE model. This section reports results of our model to model benchmark comparisons.

In all of the tests fuel moisture was held constant. Unless otherwise specified, wind direction was from 180 degrees, values of EAF tested were (1, 0.66, 0.5, 0.4, 0.33), fuel model 15, a custom fuel model for mature chamise chaparral (Weise and Regelbrugge 1997), was used, and the terrain was flat. We ran FARSITE with identical inputs.

In all of the figures in this section, FARSITE perimeters are represented as black lines and HFire perimeters as colors representing regular intervals of fire progression. Sørensen metric values quantitatively comparing HFire and FARSITE burned area at the final time step (S_f) for each model run are included on the figures.

5.1.2 Test of different wind speeds

This test isolates the effects of wind speed and the EAF. Twenty one separate HFire simulations were run, wind speed ranged from 0 to 20 m s^{-1}, in increments of 5 m s^{-1}. Five values of EAF were tested, except for the 0 m s^{-1} winds case, where EAF has no effect. For the 0 m s^{-1} wind speed simulations, Fuel Model 1, grassland, was used in order to increase rate of spread so the figure is less pixilated.

The results of this test are presented in Figures 1 and 2. As wind speed increases the fires become larger, and the length/width ratio decreases (Figure 1). The one dimensional, forward rate of spread is identical in all cases for HFire and FARSITE, the difference is in the flanking rate of spread and the resulting two dimensional shape. FARSITE produces a rounded fire front while HFire exhibits a triangular leading edge, as discussed above. Here the increasingly sharp triangular edge corresponds to an increasingly stretched vertex of the eight sided fire perimeter with increasing wind speed. The back edge of the perimeter corresponds to the remaining six sides of the eight sided figure, and has flat edges, though it appears rounded because they are close together.

In order to minimize the difference between HFire and FARSITE results, we ran HFire with five different values of EAF. Setting EAF to 1.0 corresponds to no adjustment;

values less than 1.0 decrease the length/width ratio, increasing the flanking rate of spread (Eqn 5). An EAF of 0.4 maximized the Sørensen metric between HFire and FARSITE at lower wind speeds. An EAF setting of 0.5 maximized the metric at higher wind speeds.

Figure 2 illustrates the special case of 0 m s^{-1} winds, in which the fire spreads in a circular pattern. Both HFire and FARSITE accurately capture the expected one dimensional Rothermel rate of spread, which in this case describes the radius of the expanding burn area. For FARSITE the shape is a circle, which is easily captured by the double ellipse formulation of the vector algorithm. The raster based HFire algorithm approximates the circular shape with an eight sided figure, in this case a perfect octagon.

#Insert Figure 1 Approximately Here#

#Insert Figure 2 Approximately Here#

5.1.3 Test of time varying wind direction

This test isolates the effect of varying wind direction and EAF. Thirty HFire simulations were run. Five values of EAF were tested with 6 wind azimuths: winds having a constant azimuth of 180 degrees and five different wind azimuth scenarios, listed in Table 2. For the first four scenarios the wind direction is periodically and deterministically varied by fixed increments about the 180 degree average. In the last scenario the wind direction switches between due north and due south. Wind speed was 5 m s^{-1}.

Figure 3 shows that varying the wind inputs leads to HFire and FARSITE perimeters having closer agreement. Comparing the results of Wind Azimuth Scenario 1 (Figure 3b) with those from the constant azimuth case (Figure 3a) shows that perturbing the wind direction slightly (a maximum of +/- 10 degrees) widens the fire front noticeably. Wind Azimuth Scenarios 2 and 3, which perturb the wind direction a greater amount, resulted in a smooth, non-triangular fire front for HFire (Figure 3 c,d). Hence, agreement between HFire and FARSITE improved, with Sørensen metric values above 0.9. Scenario 4 systematically perturbed the wind azimuth +/- 45 degrees about 180 degrees, leading to symmetric fire perimeters at the end of the simulation for both models, and a Sørensen metric value of 0.947 for an EAF of 0.4. Likewise, perturbing the wind +/- 180 degrees lead to symmetric shapes for both models, with a high Sørensen metric value of 0.942 (Figure 4f).

#Insert Table 2 Approximately Here#

#Insert Figure 3 Approximately Here#

5.1.4 Test of different wind speeds and slopes, with up slope winds

This test combines the effects of changing both wind speed and slope. Twenty four HFire and FARSITE simulations were run, with slopes (rise over run) of 0, 20, 40, 60, 80, and 100% and constant wind speeds of 0, 2.5, 5, and 7.5 m s^{-1}. HFire was run with the EAF set to 0.5. The wind azimuth of 180 degrees was up slope. A fire burning uphill spreads faster as the heat from the fire front preheats the adjacent fuel, driving off vegetation moisture, reducing the energy required to raise the temperature of the fuel to ignition.

Starting from the case of zero wind speed and zero slope, for our chosen increments, increasing wind speed has a greater effect on forward rate of spread than does increasing the slope by approximately a factor of two (Figure 4). Steepening the slope has a large effect on forward rate of spread at low wind speeds, but the effect at higher wind speeds is reduced. In all cases, forward rate of spread is comparable between HFire and FARSITE, with FARSITE exhibiting greater spread on the flanks of the fire.

#Insert Figure 4 Approximately Here#

5.1.5 Test of different slopes and cross-slope winds

This test combines the effects of changing slope and temporally varying wind direction. It is similar to the previous test with different wind speeds and slopes, with the modification that the wind direction is cross-slope. We tested two wind direction scenarios: winds from 270 degrees and winds from 270 degrees systematically perturbed +/- 20 degrees. Only 7.5 m s^{-1} wind speed model runs are presented. HFire was run with the EAF set to 0.5.

This test shows the largest difference between FARSITE and HFire perimeters as measured by the Sørensen metric. Differences arise because of the vector/raster differences in the models. As the slope becomes steeper, the direction of fire propagation smoothly rotates from 90 degrees to approximately 60 degrees in the FARSITE simulations (Figure 5). HFire suffers from some distortion when the direction of fire spread is not aligned with one of the eight cardinal directions of the underlying lattice--the angles to the 8 adjacent pixels. For the 0, 20, and 40% model runs, the true direction of fire propagation was approximately 90 degrees, so the HFire modeled perimeters are reasonable. For the 60 and 80% slope runs, HFire modeled the true direction of spread of approximately 75 degrees as a mixture of spread at 45 and 90 degrees. For the 100% slope, HFire modeled the true direction of spread (approximately 60 degrees) as propagating towards 45 degrees. Hence, agreement between modeled fire shapes is relatively poor (Sørensen metric values less than 0.8) for the 60, 80, and 100% slope comparisons. However, as demonstrated in the test of time varying wind direction (Section 5.1.3), perturbing the wind azimuth +/- 20 degrees about 270 degrees results in a more rounded fire front, leading to much closer agreement between the predicted fire shapes. The Sørensen metric values at the end of the simulation for the 60, 80, and 100% slope cases, where disagreement between FARSITE and HFire is highest, are 0.785, 0.718, and 0.669 for the constant 270 azimuth case but increase to 0.904, 0.909, and 0.848 for the 270 +/- 20 azimuth case.

#Insert Figure 5 Approximately Here#

5.1.6 Test of different fuel model transitions

This test isolates the effects of fuel model transitions and the EAF. Twenty HFire simulations were run. Five values for the EAF with four different landscape scenarios: a landscape solely comprised of Fuel Model 15, and Fuel Model 15 with an inset block of three different fuel models (unburnable, a synthetic fuel model based on Fuel Model 15 but with reduced fine fuel loads so that it burns more slowly than Fuel Model 15, and Fuel Model 1, grassland, which results in faster fire spread). Wind speed was 7 m s^{-1}.

The case involving homogeneous fuels exhibits the expected pattern of equivalent forward rate of spread, with FARSITE producing a wider fire front (Figure 6a). In the case involving the unburnable block the fire perimeters for both models are unchanged, except for in the block (Figure 6b). The case with the slower burning block shows, once again, that more heterogeneous conditions produced a closer match between HFire and FARSITE. For the EAF of 0.4 model run, the flanking fire spread for HFire on the left side of the fire (where two different fuels are encountered) is less than one hour behind FARSITE whereas on the right flank it is more than one hour behind (Figure 6c). The scenario where a faster burning block of fuel is encountered exhibited the strongest agreement. Unlike the cases involving the unburnable and slow burning blocks, agreement in fire spread on both flanks of the fire improved upon encountering the different block of fuels, and final Sørensen metric values were greater than 0.9. Sørensen metric values were lower for the other three scenarios due to the triangular fire front.

#Insert Figure 6 Approximately Here#

5.2 Historical fires

This section tests agreement between HFire, FARSITE, and reference fire perimeters when wind, fuels, and terrain vary under actual burning conditions. The initial stages of two historical chaparral fires were simulated. The Day Fire burned slowly for a month in Southern California in 2006. The Simi Fire was part of a complex of fires burning under Santa Ana conditions in Southern California in late October of 2003. The initial stages of the Day Fire are presented first to demonstrate a relatively simple scenario involving low wind speeds that is intermediate in complexity between the synthetic landscapes and the more complex Simi Fire. Simulations of the Calabasas Fire, a short lived Santa Ana wind driven event, are presented as supplementary online material.

Two types of comparisons are made in this section: model to model, and both HFire and FARSITE models to measured perimeters. Model to model comparisons under realistic burning conditions serve as further benchmarks of HFire. Comparisons between the models and perimeters serve to build understanding and gain confidence. The accuracy of predicted perimeters is limited by the underlying semi-empirical/semi-physical nature of the Rothermel equations, the spatial resolution of the landscape variables, and the temporal (hourly) and spatial (point) resolution of the wind data. Furthermore, historical fire suppression information is often not available or available in a way that is easily incorporated into the models. Finally, the accuracy of the reference historical fire perimeters varies and may not be the absolute standard needed. Hence, the primary benefit of the models vs. reality comparisons lies in developing a general understanding of fire modeling, and defining future directions for model refinement to improve model accuracy and predictive power.

5.2.1 Day Fire

The Day Fire was reported at 1355 hours on 4 September 2006 and was contained on 2 October 2006. It burned 65,871 ha, and cost $73.5 million to suppress. The fire initially spread slowly, burning only 5,000 ha by 9 September. Major wind driven runs occurred on the 12th, 16th – 19th, 22nd – 24th, and 27th of September. Only the first 58 hours of burning (1400 hours 4 September – 2300 hours 6 September) are simulated as both fire spread models dramatically over predict initial fire growth, due to effective fire suppression efforts at the initial stages of the actual event.

The Day Fire burned through a southern California chaparral/coastal sage scrub (CSS) mosaic. The state of California Fire and Resource Assessment Program (FRAP) map was used to determine fuel models. Two different sets of fuel models were used to characterize the vegetation (Table 3): the fuel models developed by Anderson (1983), formally called the Northern Forest Fire Lab (NFFL) models; and custom fuel models that were specifically developed for chaparral, the Riverside Fire Lab (RFL) fuel models (Weise and Regelbrugge 1997). The 1-, 10-, and 100-hour fuel size classes of Table 3 correspond to <¼, ¼-1, and 1-3 inch diameter woody material, and are based on how quickly dead fuel moisture responds to changes in atmospheric relative humidity.

#Insert Table 3 Approximately Here#

The 30m FRAP fuels map uses NFFL fuel models, however the fuel models for shrubs were changed to the RFL chaparral fuel models for this analysis. NFFL Fuel Model 4 was converted to RFL 16 (Ceanothus chaparral), NFFL 6 to RFL 15 (mature chamise chaparral), and NFFL 5 to RFL 18 (CSS). Fuel Models 28, 98, 15, and 97 which represent urban, water, desert, and irrigated agriculture, respectively, were reclassified to Fuel Model 99, the designated number for unburnable cells. Topographic variables were derived from a 30m USGS DEM. Slope and aspect were derived using standard techniques.

The weather data were obtained from the Cheeseboro, California RAWS station, which is located 48 km south of the final fire extent. RAWS closer to the fire were not used because data were either missing or noisy. RAWS data consist of daily precipitation, maximum/minimum temperature, maximum/minimum humidity, timing of maximum and minimum temperatures (hourly values are interpolated by FARSITE), and elevation of the weather station (needed to interpolate weather variables across the landscape, using environmental lapse rates). Live fuel moisture during the simulation was held constant at a value of 60% of oven dry weight (ODW) for live herbaceous material and 60% ODW for live woody material. Live fuel moisture in chaparral in the fall drops to the annual minimum value, which is on the order of 60% (Countryman and Dean 1979; Roberts *et al.* 2006).

5.2.1.1 Day Fire results

Both FARSITE and HFire modeled the Day Fire as having a generally circular shape, due to low wind speeds and alternating wind directions during the simulation period (Figure 7). Low wind speeds favor circular fires and from 1400 hours on 4 September to 2300 hours on 6 September, wind speeds were greater than 5 m s^{-1} only 7 of 58 hours, the maximum wind speed was 6.7 m s^{-1}, and the median wind speed was 3.1 m s^{-1}. Additionally, because the wind alternates in a typical diurnal pattern between easterly in the mornings and westerly in the afternoons, wind did not have a net directional effect on fire spread. This is similar to the varying wind direction test (Section 5.1.3), where alternating wind conditions in Wind Azimuth Scenario 5 lead to an oval fire shape. Hence, with wind speed favoring a circular shape, and wind direction favoring an oval shape, the resulting shape is generally compact and rounded for the Day Fire.

#Insert Figure 7 Approximately Here#

The effect of altering EAF clearly has a greater effect on fire size than fire shape in heterogeneous conditions. Three different values for EAF in HFire were tested, 0.5, 0.66, and 0.9. The modeled fires were all roughly circular, with the EAF 0.5 fire being largest and the EAF 0.9 fire being smallest. Lower values of the EAF in the synthetic landscapes tests are found to widen the fire front, influencing the flanking fire rate of spread only. On a realistic landscape, because the direction of maximum rate of spread is constantly changing, increasing the flanking rate of spread serves to increase the overall rate of spread, and this emerges as the most apparent result of varying EAF.

Sørensen metric values between HFire and FARSITE modeled perimeters were highest for the EAF 0.66 model run, with values generally above 0.9 for the first 2 days of burning, and above 0.8 on the third day. Complete Sørensen metric values are available as an online supplement (Supplemental Table 1). The synthetic landscape tests for HFire and FARSITE produced high values for the Sorenson metric in situations that are relevant to the Day Fire. In the synthetic landscapes, values tend to be higher at lower wind speeds and moderate slopes (Figure 4), when the wind direction alternates (Figure 3), and when fuels are more heterogeneous (Figure 6).

The superiority of the 0.66 EAF model run differs from the synthetic landscape cases where EAF values of 0.4 and 0.5 were superior (a greater EAF was needed to widen the fire shape in the homogeneous cases). The varying wind azimuth (section 5.1.3) and fuel model (section 5.1.6) tests demonstrated that HFire shapes become less angular under shifting conditions. In actual fire conditions, where landscape and wind are varying simultaneously, the combined effect is to reduce the need for the EAF (a value closer to 1.0 can be used).

Simulations of the Day fire demonstrate that HFire and FARSITE produce similar fire perimeters under low wind conditions. These weather conditions during the early portion of the fire were amenable to successful fire suppression efforts, and the fire was actively suppressed. Supplemental Figure 1 shows the final HFire and FARSITE perimeters are approximately five times larger than a perimeter derived from the MODIS active fire product. A convex hull polygon was generated from the set of all active fire cells (current and past) for the Day Fire as of 6 September.

5.2.2 Simi Fire

The Simi Fire burned from October 25 to November 5, 2003, consumed 44,000 ha, destroyed 315 structures, and cost approximately $10 million to suppress. It was a Santa Ana wind driven fire, which exhibited rapid westward growth on the 26th of October due to high wind speeds. The first 34 hours of the fire were simulated, from 1300 hours on 25 October to 2300 hours on 26 October.

The Simi Fire burned through a southern California chaparral/grassland mosaic. The State of California FRAP Map was used to determine fuel models as described above for the Day Fire. Topographic variables were derived from a 30m USGS DEM, slope and aspect were derived using standard techniques. Weather data was obtained from the Cheeseboro, California RAWS Station, located 8 km south of the central portion of the final fire extent.

Accuracy was assessed using perimeters derived from the MODIS active fire product, which uses data from both the Aqua and Terra satellites. It is produced 4 times a day, at 1km cell resolution. Convex hull polygons were generated from the set of all active fire cells (current and past) for each time step. These polygons were then clipped using the official final fire perimeter from the California Department of Forestry and Fire Prevention (CDF) to remove the presence of false positives in the MODIS product.

The Simi Fire was chosen for simulation because it is representative of fires in chaparral, experiencing high wind speeds and high rates of spread.

5.2.3.1 Simi Fire results

Figure 8 shows HFire and FARSITE perimeters from 25 October 1400 hours to 26 October 2300 hours. HFire is shown for an EAF of 0.66, which again provided the highest overall agreement. The shapes of initial fire progression to the southwest are very similar, with rate of spread slightly faster for FARSITE. The flanking rate of spread was slightly faster for HFire. The HFire simulation reached the western edge of Simi Valley ('b' on Figure 8) at 0900 hours on 26 October whereas the FARSITE simulation reaches the same landmark at 1200 hours. Other features of note include the expansion of HFire perimeters into areas that FARSITE did not burn, to the north and to the west (marked a and b on Figure 8). HFire was better able to utilize narrow corridors to reach additional areas of fuel. FARSITE was run with a perimeter resolution of 99m. Finer resolutions have been evaluated in previous research on the Simi Fire (Peterson *et al.* 2005) but result in very long model run times for FARSITE (on the order of 3-7 days) and the finest resolution that the model was successfully run at was 59m. This is twice the resolution at which HFire was run, 30m, which is the native resolution of the landscape variables. Fire spread in the south central portion of the fire, marked c on Figure 8, further illustrates this point. Both HFire and FARSITE show fire just north of point c at 1700 hours on 25 October. HFire propagated fire to the southwest during the next hour, whereas FARSITE required five hours to get through the corridor. This has implications for fires in the wildland urban interface (WUI) where narrow corridors may be common. Despite these areas of disagreement, Sørensen metric values were again high, generally on the order of 0.85 – 0.9, because of the large area in the main body of the fire which overlaps for the two models. Complete Sørensen metric values are available as an online supplement (Supplemental Table 2).

#Insert Figure 8 Approximately Here#

Figure 9 shows HFire, FARSITE, and MODIS derived perimeters at two times, 2300 hours on 25 October for the models and 2233 hours on 25 October for MODIS, and 1200 hours on 26 October for the models and 1209 hours on 26 October for MODIS. For the first comparison, the HFire and FARSITE perimeters were nearly identical on the east and west flanks of the fire. However, HFire exhibited greater spread to the southwest. Both modeled perimeters agreed well with MODIS (Sørensen metric values on the order of 0.75). The value for HFire was slightly lower because of over burning to the southwest. Fire suppression during the Simi Fire is only anecdotally documented, but as mentioned in the previous paragraph, the area of over burning by HFIRE at point c is separated from the main body of the landscape by a narrow corridor, so fire suppression efforts could have been focused on the small area, enhancing success. Additionally, MODIS resolution is course at 1km, so the precision of the MODIS shape is uncertain.

#Insert Figure 9 Approximately Here#

For the second comparison, the modeled fires and the actual fire have reached the farthest western extent of the Simi Fire. HFire over burned farther to the west, while FARSITE was not able to negotiate the narrow fuel corridors to the west. Both modeled fires also over burn to the south and the southeast. This over burning of modeled fires relative to the MODIS perimeter likely reflects the presence of active fire suppression. Again, anecdotal information suggests that fire suppression was active to the south owing to the presence of the Ronald Reagan Presidential Library and other areas of high value real estate. Sørensen metric values are lower for this comparison, due to over burning.

Simulations of the Simi Fire demonstrate that HFire and FARSITE produce generally similar fire perimeters, though HFire is better able to negotiate narrow fuel corridors in the terrain. The general location of the modeled fire fronts with respect to MODIS was good, though the fire spread models, which do not include information about fire suppression, tend to over predict areas of fire spread.

5.3 Run time efficiency

Run time efficiency is an important attribute of a fire spread model, both for the simulation of individual fires and simulations of long term fire regimes. Similar to other raster models, the performance of HFire is proportional to the number of ignited cells and the rate of spread of the fastest burning cell. In contrast, FARSITE model performance is a function of the user specified simulation resolution, the heterogeneity of the conditions through which the fire is burning (highly heterogeneous conditions increase the number of sub-time steps in a time step), and the complexity of the fire perimeter crossovers, mergers, and islands resolved during the fire perimeter discretization process.

The run time performance of HFire was evaluated relative to FARSITE for each of the historical fire simulations described in this paper. All of the simulations used in the timing analysis were performed on a PC with an Intel Core2 Duo dual-core processor, 2 gigabytes of RAM, and running the Windows XP 32-bit operating system. Care was taken to ensure that the simulation was the only active task not associated with the operating system on the computer.

The wall clock times required to simulate 58 hours of the Day Fire, 12 hours of the Calabasas Fire (online supplemental text), and 35 hours of the Simi Fire were recorded. All FARSITE simulations were performed with perimeter and distance resolution set to 99m. Values closer to the native resolution (30 m) of the input terrain and fuels significantly increase the run time without a substantial increase in accuracy (Peterson *et al.* 2005). HFire (6.33 min) completed the simulation of the Day Fire approximately 2.3 times faster than FARSITE (14.83 min). The relatively small difference can be attributed to the relatively homogeneous landscape and low wind conditions used as inputs to these simulations. The Calabasas Fire is more complex, involving varying terrain and fuels and higher wind speeds. HFire (1.1 min) completed the simulation approximately 8 times faster than FARSITE (8.75 min). The Simi Fire was the most complex simulation, covering the largest area. HFire (6.1 min) completed the simulation approximately 162 times faster than FARSITE (16.5 h).

Figure 10 illustrates model run times for each hour of the Simi Fire with cumulative area burned (x-axis) plotted versus HFire and FARSITE run times on separate y-axes. The trend for HFire is approximately linear, which implies that the run time is proportional to the number of ignited cells. The trend for FARSITE is more complex. It is approximately linear from the time of ignition until 30,000 ha burned, which occured at 200 hours on 26 October. During this initial period the fire shape was relatively simple (Figure 8). The period from 400 to 1300 hours on 26 October exhibits the steepest slope (longest model run time in comparison to the net area burned). During this period the perimeter length and complexity increased relative to the area burned as the fire expanded to the south and southeast (points c and d on Figure 8). The increased perimeter length leads to longer calculation times because more vertices are added to the perimeter to meet the specified perimeter resolution. The inset on the main graph of Figure 10, a log-log plot of run time vs. area burned, emphasizes these findings. Initial differences in run time between HFire and FARSITE for the Simi Fire are of the same order of magnitude as for the Calabasas Fire: at the fourth hour, HFire burned 10^4 ha in less than one minute, FARSITE in just under 10 minutes. The longer computation rates for FARSITE at later points in the simulation period are clearer because both model run times are plotted on the same axis.

#Insert Figure 10 Approximately Here#

6. Conclusions

The 2003 and 2007 Southern California Wildfires have raised public awareness of the impact of wildfires on urban communities and increased concerns about potential future fire hazards associated with climate change. Given how little we know about climate change impacts on fire probabilities (Moritz and Stephens in press) and the importance of fire spread models as the basis of simulating ecological disturbance regimes, new and more physically based approaches are needed. The computational efficiency of the HFire algorithm creates opportunities for mechanistic fire models to play quantitative and dynamic roles in analysis of fire patterns. HFire improves on existing raster models of fire spread in two important ways. First, the adaptive time step is an elegant alternative to fixed interval models because the simulation clock responds to the fire behavior and increments more slowly during periods of rapid fire spread and more rapidly under moderate fire spread. The second major advance of HFire is to allow fire spread to occur in distance increments smaller than the cell size. Because of this, a cell is ignited by accumulating the distance spread from all eight directions and over multiple time steps. The cumulative benefit of these features is to reduce the distorted geometries associated with other raster models.

To evaluate performance and improve understanding of optimal parameterization, we compared HFire to FARSITE over a series of synthetic landscapes with varying conditions and for three actual fires.

Predictions from HFire were similar to those obtained from FARSITE for a standard set of benchmarks developed by Finney (1998) and used during the testing of the

FARSITE model. Although the predictions from HFire and FARSITE for the benchmarks are virtually identical in the direction of the maximum rate of fire spread, there are differences between the models for fire spread along the flanks. The raster distortion that is observed in some of the predictions from HFire for the benchmarks on homogeneous landscapes is not apparent in the simulations of historical fires.

In the historical fire accuracy assessment, a key advantage of the HFire algorithm—numerical efficiency and robustness—clearly emerges. Several additional observations are made based on the historical simulations. First, comparisons of fire spread are complicated by the impact of fire suppression. Both the Day and Calabasas fires were modeled as being much larger than the actual fires. Both models also overpredict burn area for the Simi Fire, due to active fire suppression along the southern portion of the fire, though this had less of an effect on accuracy due to the large amount of unburnable fuels in the path of the fire. Second, predicted fire spread from both models is highly influenced by the meteorological data used, and in particular the wind speed and direction. Third, the results from the Simi Fire showed that HFire is better able to negotiate fire spread through narrow corridors of fuel typically associated with the wildland urban interface (WUI). More research is needed to verify and understand the impact of this finding.

Analysis of these results support the promise and utility of fire models as a tool for wildland management, policy and hazard estimation. At the same time, certain systematic discrepancies between both of the models and the perimeters of historical fires suggest important future directions for wildfire modeling which will increase the fidelity of the model results. Acquiring wind data at finer spatial and temporal resolution is suggested. Accounting for fire suppression in a deterministic manner would also be beneficial. Future enhancements of HFire may include: (i) modification of the fire spread equation and rules, (ii) addition of a spotting module, (iii) addition of a suppression module that allows for scenario testing, (iv) higher resolution temporal inputs for wind and fuel moisture, and (v) representations of fuel treatment and type conversion.

In summary, HFire represents an improvement over current models because it provides a similar level of accuracy with orders of magnitude improvement in computation time. The increased algorithmic efficiency has many ramifications. It makes possible near real time estimates of fire spread, such as might be available in a mobile or other embedded device that can be worn by fire fighters on the fire line. It allows for simulations of longer, larger fires, such as the Simi Fire. Additionally a quantitative estimate of fire risk could be obtained for a locale by testing hundreds of different fuel treatment, fuel moisture, and fire suppression scenarios under different weather conditions (e.g. Finney 2001). Finally, HFire is ideal for mechanistic simulation of long term fire regimes under different climate change and WUI expansion scenarios, enhancing our ability to understand underlying controls on fire patterns and to mitigate the effect of anthropogenic changes.

7. Acknowledgements

This work was supported by the James S. McDonnell Foundation, the David and Lucile Packard Foundation, NSF Grant DMR-0606092, the Institute for Collaborative

Biotechnologies through ARO grants DAAD19-03-D-0004, and a National Aeronautics and Space Administration (NASA) Regional Earth Science Application Center grant (CSDH NASA RESAC 447633-59075).

8. References

Albini FA (1976) 'Estimating wildfire behavior and effects.' USDA Forest Service, Intermountain Forest and Range Experiment Station General Technical Report GTR-INT-30. (Ogden, UT)

Albini FA, Baughman RG (1979) 'Estimating wind speeds for predicting wildland fire behavior.' USDA Forest Service, Intermountain Forest and Range Experiment Station Research Paper RP-INT-221. (Ogden, UT)

Albini FA, Chase CH (1980) 'Fire containment equations for pocket calculators.' USDA Forest Service, Intermountain Forest and Range Experiment Station Research Paper RP-INT-268. (Ogden, UT)

Anderson DG, Catchpole EA, DeMestre NJ, Parkes E (1982) Modeling the spread of grass fires. *Journal of the Australian Mathematical Society: Series B – Applied Mathematics* **23**, 451-466.

Anderson HE (1983) 'Predicting wind-driven wildland fire size and shape.' USDA Forest Service, Intermountain Forest and Range Experiment Station Research Paper RP-INT-305. (Ogden, UT)

Andrews PL (1986) 'BEHAVE: Fire Behavior Prediction and Fuel Modeling Subsystem-BURN Subsystem, Part 1.' USDA Forest Service, Intermountain Forest and Range Experiment Station General Technical Report GTR-INT-194. (Ogden, UT)

Beer T (1990) The Interaction of Wind and Fire. *Boundary-Layer Meteorology* **54**, 287-308.

Berjak SG, Hearne JW (2002) An improved cellular automaton model for simulating fire in a spatially heterogeneous Savanna system. *Ecological Modeling* **148**, 133-151.

Burgan RE, Rothermel RC (1984) 'BEHAVE: Fire Behavior Prediction and Fuel Modeling System--FUEL Subsystem.' USDA Forest Service, Intermountain Forest and Range Experiment Station General Technical Report GTR-INT-167. (Ogden, UT)

Butler BW, Finney M, Bradshaw L, Forthofer J, McHugh C, Stratton R, Jimenez D (2006) WindWizard: A New Tool for Fire Management Decision Support. In 'Fuels Management—How to Measure Success: Conference Proceedings.' USDA Forest Service, Rocky Mountain Research Station Proceedings RMRS-P-41. (Fort Collins, CO)

Catchpole T and DeMestre N (1986) Physical models for a spreading line fire. *Australian Forestry* **49**, 102-111.

Clark RE, Hope AS, Tarantola S, Gatelli D, Dennison PE, Moritz MA (in press) Sensitivity analysis of a fire spread model in a chaparral landscape. *Fire Ecology.*

Clarke KC, Brass JA, Riggan PJ (1994) A cellular automaton model of wildfire propagation and extinction. Photogrammetric *Engineering and Remote Sensing* **60**, 1355-1367.

Countryman CM, Dean WH (1979) ‘Measuring moisture content in living chaparral: A field user's manual.’ USDA, Forest Service, Pacific Southwest Forest and Range Experiment Station General Technical Report GTR-PSW-36. (Berkeley, CA)

Dennison PE, Roberts DA, Thorgusen SR, Regelbrugge JC, Weise D, Lee C (2003) Modeling seasonal changes in live fuel moisture and equivalent water thickness using a cumulative water balance index. *Remote Sensing of Environment* **88**, 442-452.

Dennison PE, Roberts DA, Peterson SH, Rechel J (2005) Use of normalized difference water index for monitoring live fuel moisture. *International Journal of Remote Sensing* **26**, 1035-1042.

Finney MA (1998) ‘FARSITE: Fire Area Simulator- model development and evaluation.’ USDA Forest Service, Rocky Mountain Research Station Research Paper RP-RMRS-4. (Ft. Collins, CO)

Finney, MA (2001) Design of regular landscape fuel treatment patterns for modifying fire growth and behavior. *Forest Science* **47**, 219–228.

Fons WL (1946) Analysis of fire spread in light fuels. *Journal of Agricultural Research* **72**, 93-121.

Frandsen WH, Andrews PL (1979) ‘Fire behavior in nonuniform fuels.’ USDA Forest Service, Intermountain Forest and Range Experiment Station Research Paper RP-INT-232. (Ogden, UT)

French IA, Anderson DH, and Catchpole EA (1990) Graphical Simulation of Bushfire Spread *Mathematical Computer Modelling* **13**, 67-71.

Green DG (1983) Shapes of Simulated Fires in Discrete Fuels. *Ecological Modeling* **20**, 21-32.

Green DG, Tridgell A, Gill MA (1990) Interactive simulation of bushfires in heterogeneous fuels, *Mathematical and Computer Modelling* **13**, 57-66.

Greig-Smith P (1983) 'Quantitative Plant Ecology.' 3rd edn. (University of California Press: Berkeley, CA)

Hanson HP, Bradley MM, Bossert JE, Linn RR, Younker LW (2000) The potential and promise of physics-based wildfire simulation. *Environmental Science and Policy* **3**, 171-172.

Hargrove WW, Gardner RH, Turner MG, Romme WH, Despain DG (2000) Simulating fire patterns in heterogeneous landscapes. *Ecological Modeling* **135**, 243-263.

Kourtz PH, O'Regan WG (1971) A model for a small forest fire, to simulate burned and burning areas for use in a detection model. *Forest Science* **17**, 163-169.

Linn RR (1997) A transport model for prediction of wildfire behavior. Ph.D. dissertation, New Mexico State University, Los Alamos National Laboratory Thesis LA-13334-T. 195pp.

Linn RR, Reisner J, Colman, J J, Winterkamp J (2002) Studying wildfire behavior using FIRETEC. *International Journal of Wildland Fire* **11**, 233-246.

Morais M (2001) Comparing Spatially Explicit Models of Fire Spread Through Chaparral Fuels: A New Algorithm Based Upon the Rothermel Fire Spread Equation. MA Thesis, University of California Santa Barbara, Santa Barbara, CA.

Moritz MA, Morais ME, Summerell LA, Carlson JM, Doyle J (2005) Wildfires, complexity, and highly optimized tolerance. *Proceedings of the National Academy of Sciences of the United States of America* **102** (50), 17912-17917.

Moritz MA, Stephens SL (in press) Fire and sustainability: considerations for California's altered future climate. *Climatic Change*.

Nelson RM, Adkins CW (1988) A dimensionless correlation for the spread of wind-driven fires. *Canadian Journal of Forest Research* **18**, 391-397.

Ntaimo, L., B.P. Zeigler, M.J. Vasconcelos and B. Khargharia (2004) Forest Fire Spread and Suppression in DEVS. *SIMULATION: Transactions of the Society for Modeling and Simulation International*, 80(10), 479-500.

Perry GLW, Sparrow AD, Owens IF (1999) A GIS-supported model for the simulation of the spatial structure of wildland fire, Cass Basin, New Zealand. *Journal of Applied Ecology* **36**, 502-518.

Peterson SH, Goldstein NC, Clark ML, Halligan KQ, Schneider P, Dennison PE, and Roberts DA (2005) Sensitivity Analysis of the 2003 Simi Wildfire Event. In '*Proceedings, Geocomputation 2005'* (Ann Arbor, Michigan)

Pitts WM (1991) Wind effects on fires *Progress Energy Combustion Science*. **17**,83-134.

Richards GD (1990) An Elliptical Growth Model Of Forest Fire Fronts And Its Numerical Solution *International Journal for Numerical Methods in Engineering* **30**, 1163-1179.

Roberts DA, Dennison PE, Peterson SH, Sweeney S, Rechel J (2006) Evaluation of AVIRIS and MODIS measures of live fuel moisture and fuel condition in a shrubland ecosystem in southern California. *Journal of Geophysical Research – Biogeosciences* **111**, G04S02.

Rothermel RC (1972) ‘A mathematical model for predicting fire spread in wildland fuels.’ USDA Forest Service, Intermountain Forest and Range Experiment Station Research Paper RP-INT-115. (Ogden, UT)

Rothermel RC (1983) ‘How to predict the spread and intensity of forest and range fires.’ USDA Forest Service, Intermountain Forest and Range Experiment Station General Technical Report GTR-INT-143. (Ogden, UT)

Rothermel RC, Wilson RA, Morris GA, Sackett SS (1986) ‘Modeling moisture content of fine dead wildland fuels: Input to the BEHAVE fire prediction system.’ USDA Forest Service, Intermountain Forest and Range Experiment Station, Research Paper RP-INT-359 (Ogden, UT)

Rothermel, RC (1991) ‘Predicting the behavior and size of crown fires in the northern Rocky Mountains.’ USDA Forest Service, Intermountain Forest and Range Experiment Station, Research Paper RP-INT-438 (Ogden, UT)

Weber RO (1991) Modeling fire spread through fuel beds. *Progress in Energy and Combustion Science* **17**,67-82.

Weise DR and Regelbrugge JC (1997) Recent chaparral fuel modeling efforts, submitted to California Fuels Committee Newsletter. Prescribed Fire and Fire Effects Research Unit, Riverside Fire Laboratory, Pacific Southwest Research Station. 3p.

Williams FA (1976) Mechanisms of Fire Spread. In ‘Proceedings 16th Symposium on Combustion.’ pp. 1281-1294. (The Combustion Institute: Pittsburgh, PA)

Table 1. Variables required for predicting fire spread using HFire. Italicized variables require a value for each of the following size classes: dead 1-hour (<0.635 cm diameter), dead 10-hour (0.635-2.54 cm diameter), dead 100-hour (2.54-7.62 cm diameter), live herbaceous, and live woody fuels.

Fuel Variables

Variable	Units
fuel load	kg m^{-2}
surface area to volume (σ)	m^2 m^{-3}
heat content	J kg^{-1}
total silica content	%
effective silica content	%
fuel bed depth	m
moisture of extinction	%

Terrain Variables

Variable	Units
elevation	m
slope	%
aspect	degrees azimuth

Environmental Variables

Variable	Units
dead fuel moisture	%
live fuel moisture	%
wind speed	m s^{-1}
wind direction	degrees azimuth

Table 2. Scenarios for alternating wind azimuth conditions. The first three involve perturbations from 180 degrees. The last two involve alternating wind directions.

	Hour								
Scenario	0	1	2	3	4	5	6	7	8
1	180	190	170	185	175	180	190	170	180
2	180	210	150	195	165	180	210	150	180
3	200	220	170	210	130	190	220	140	180
4	180	225	135	225	135	225	135	180	180
5	180	360	180	360	180	360	180	360	180

Table 3. Biomass and fuel bed height for the fuel models used in this study.

		Fuel Biomass (Mg/ha)					
		Dead			Live		
Fuel Model	Fuel Model Description	1 hr	10 hr	100 hr	Herbaceous	Woody	Fuel Bed Depth (cm)
NFFL 1	grass	1.66	0	0	0	0	30.48
NFFL 2	savana	4.49	2.25	1.12	0	1.12	30.48
NFFL 4	shrub	11.25	9.01	4.49	0	11.25	182.88
NFFL 5	shrub	2.25	1.12	0	0	4.49	60.96
NFFL 6	shrub	3.37	5.61	4.49	0	0	76.20
NFFL 8	timber	3.37	2.25	5.61	0	0	6.10
NFFL 10	timber	6.76	4.49	11.25	0	4.49	30.48
RFL 15	old chamise	4.48	6.73	2.24	1.12	4.48	91.44
RFL 16	ceanothus	5.04	10.76	4.04	6.73	6.28	182.88
RFL 18	sagebrush/buckwheat	12.33	1.79	0.22	1.68	5.6	91.44
Farsite 99	unburnable	0	0	0	0	0	0

Figure captions

Figure 1. A test of varying wind speeds on flat terrain, showing HFire (colors) and FARSITE (lines) perimeters for (a) 5 m s^{-1}, (b) 10 m s^{-1}, (c) 15 m s^{-1}, and (d) 20 m s^{-1} winds. The length/width ratio of the ellipses increases as wind speed increases. HFire shown for EAFs (*k* in Eqn 5) of 1.0, 0.66, 0.5, 0.4, and 0.33.

Figure 2. Null wind speed test on flat terrain, showing HFire (colors) and FARSITE (lines) perimeters for 0 m s^{-1} winds. The fire is circular for FARSITE and symmetrically octagonal for HFire.

Figure 3. A test of varying azimuth scenarios for 5 m s^{-1} winds, showing HFire (colors) and FARSITE (lines) perimeters for (a) constant azimuth, (b) azimuth scenario 1, (c) scenario 2, (d) scenario 3, (e) scenario 4, (f) scenario 5. There is better agreement between HFire and FARSITE modeled fire shapes as perturbations of the azimuth increase.

Figure 4. A test of varying wind speed and slope, with up slope winds, showing HFire (colors) and FARSITE (lines) perimeters. The length/width ratio of the ellipses increases as wind speed and slope steepness increase.

Figure 5. A test of 7.5 m s^{-1} wind speed, varying slope, and wind azimuth, with cross-slope winds, showing HFire (colors) and FARSITE (lines) perimeters. This test reveals raster based limitations of HFire fire spread when the direction of spread is not in a cardinal direction. This affect is mitigated when wind azimuth is perturbed.

Figure 6. A test of different blocks of fuels with 7 m s^{-1} winds, showing HFire (colors) and FARSITE (lines) perimeters for 4 fuel model (FM) maps: (a) uniform FM 15, (b) FM 15 plus unburnable, (c) FM 15 plus slower burning, (d) FM 15 plus faster burning. Increased

heterogeneity in fuels leads to better agreement between HFire and FARSITE modeled perimeters.

Figure 7. Simulated perimeters for the Day Fire, HFire shown for EAFs of (a) 0.5, (b) 0.66, (c) 0.9, and (d) FARSITE. Times are in DDHHMM format. Low wind speeds and a diurnal wind pattern lead to roughly circular fire shapes. HFire run with an EAF of 0.66 shows the best agreement with FARSITE perimeters. Associated Sørensen metric scores are listed in Supplemental Table 1.

Figure 8. Simulated perimeters for the Simi Fire for HFire (EAF 0.66) and FARSITE. Times are in DDHHMM format. Sørensen metric scores are listed in Supplemental Table 2. FARSITE propagates the fire slightly faster in the forward spread direction whereas HFire is faster in the flanking direction. Additionally, HFire is better able to navigate narrow fuel corridors, fire spread at point a and b is only present in the HFire perimeters, and fire spread at c and d occurs earlier in the HFire simulations.

Figure 9. Simi Fire perimeters, HFire (white), FARSITE (black), and MODIS reference (red), for 2 hours of the Simi Fire, 2300 hours 25 October and 1200 hours 26 October. Times are in DDHHMM format. Agreement is good for the first comparison. Agreement for the second comparison is hindered because the actual fire was actively suppressed.

Figure 10. Model run times for the Simi Fire for HFire and FARSITE, on separate axes. HFire shows a consistent relationship between fire size and model run time throughout the 6 minute burn time. The model run time is 16.5 hours for FARSITE, with run time for a particular hourly time step being dependent on the fire shape. Inset is a log-log plot of run time with HFire and FARSITE run times on the same axis to emphasize differences.

Figure 1

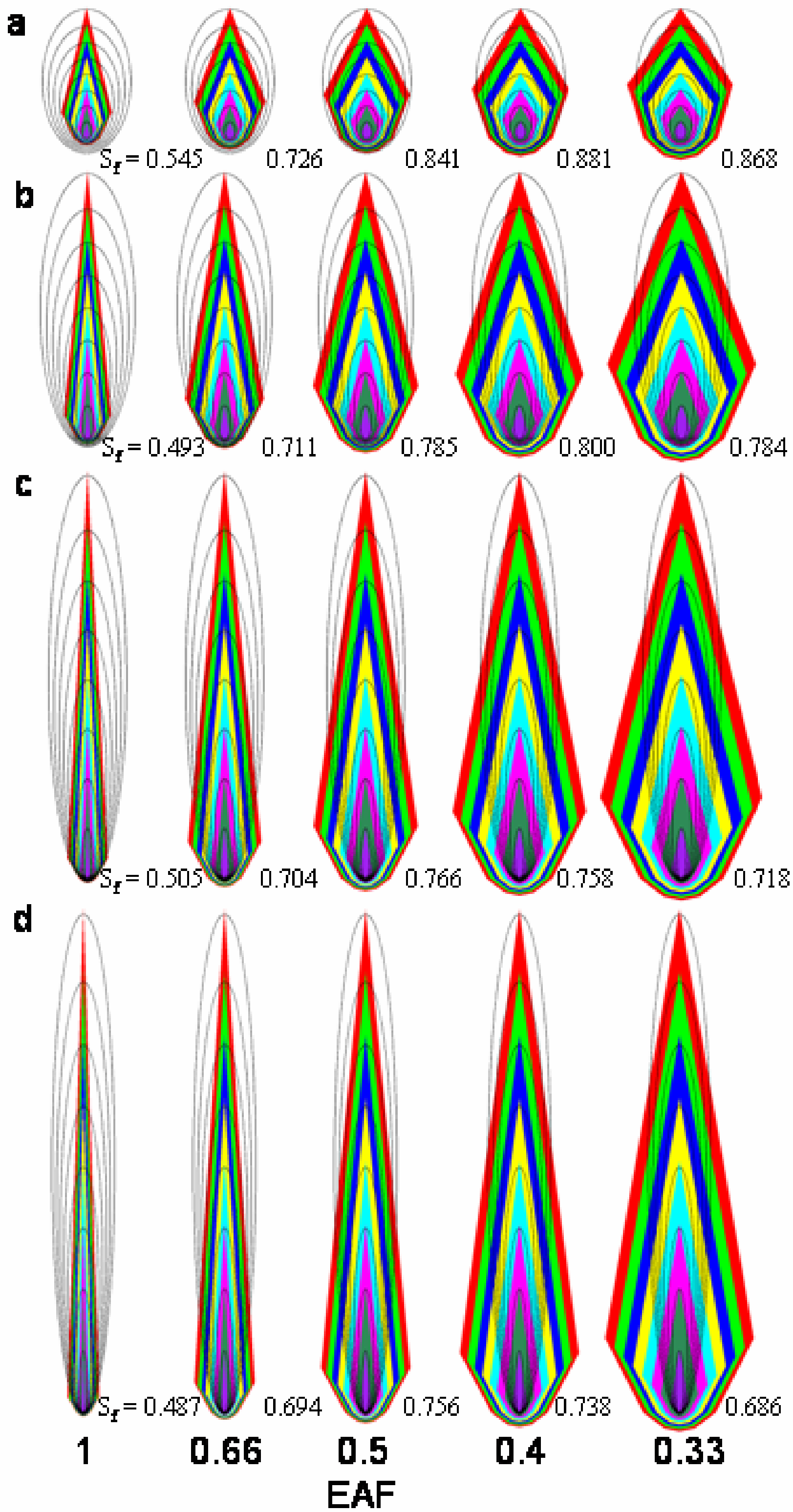
a
S_f = 0.545
0.726
0.841
0.881
0.868
b
S_f = 0.493
0.711
0.785
0.800
0.784
c
S_f = 0.505
0.704
0.766
0.758
0.718
d
S_f = 0.487
0.694
0.756
0.738
0.686
1
0.66
0.5
0.4
0.33
EAF

Figure 2

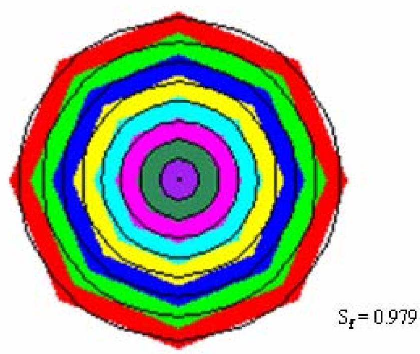

1058 Figure 3

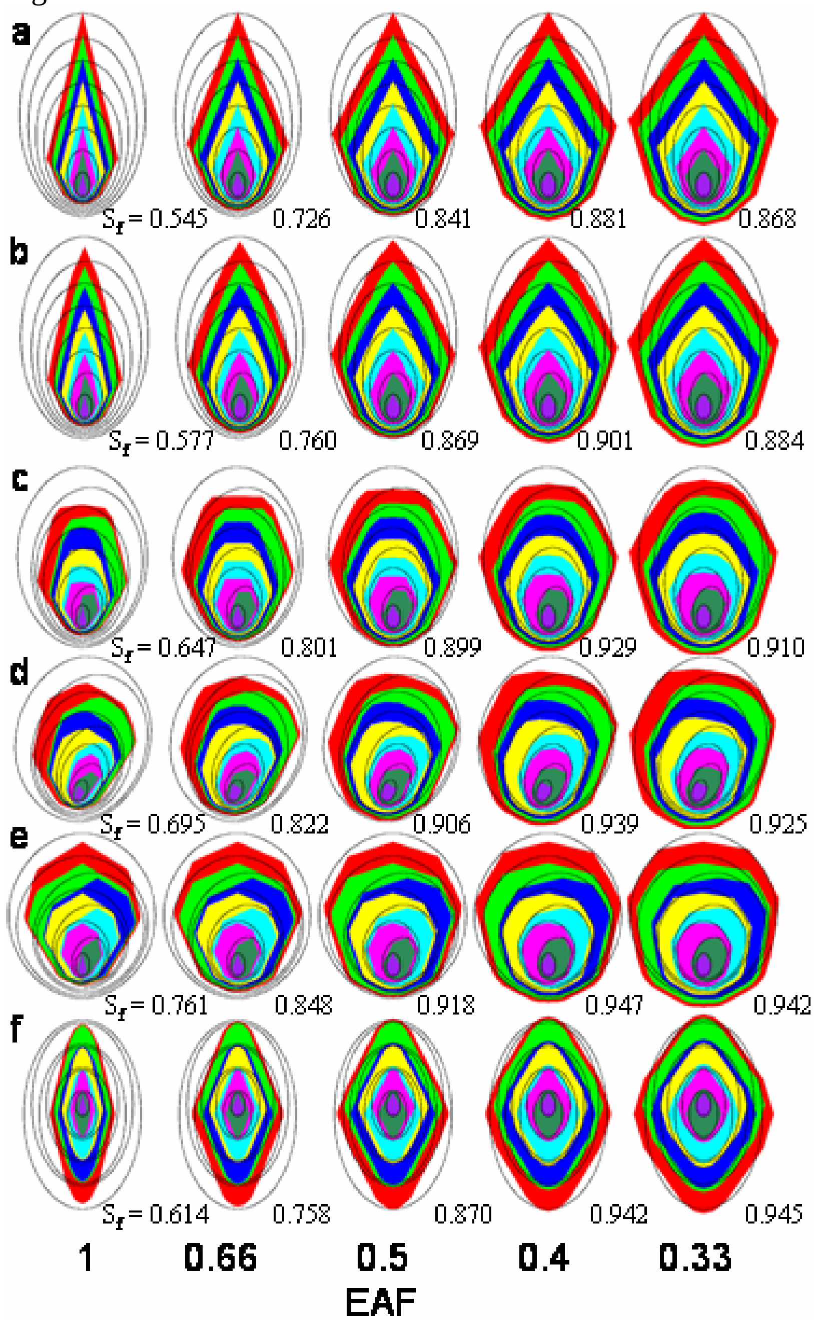

1059

Figure 4

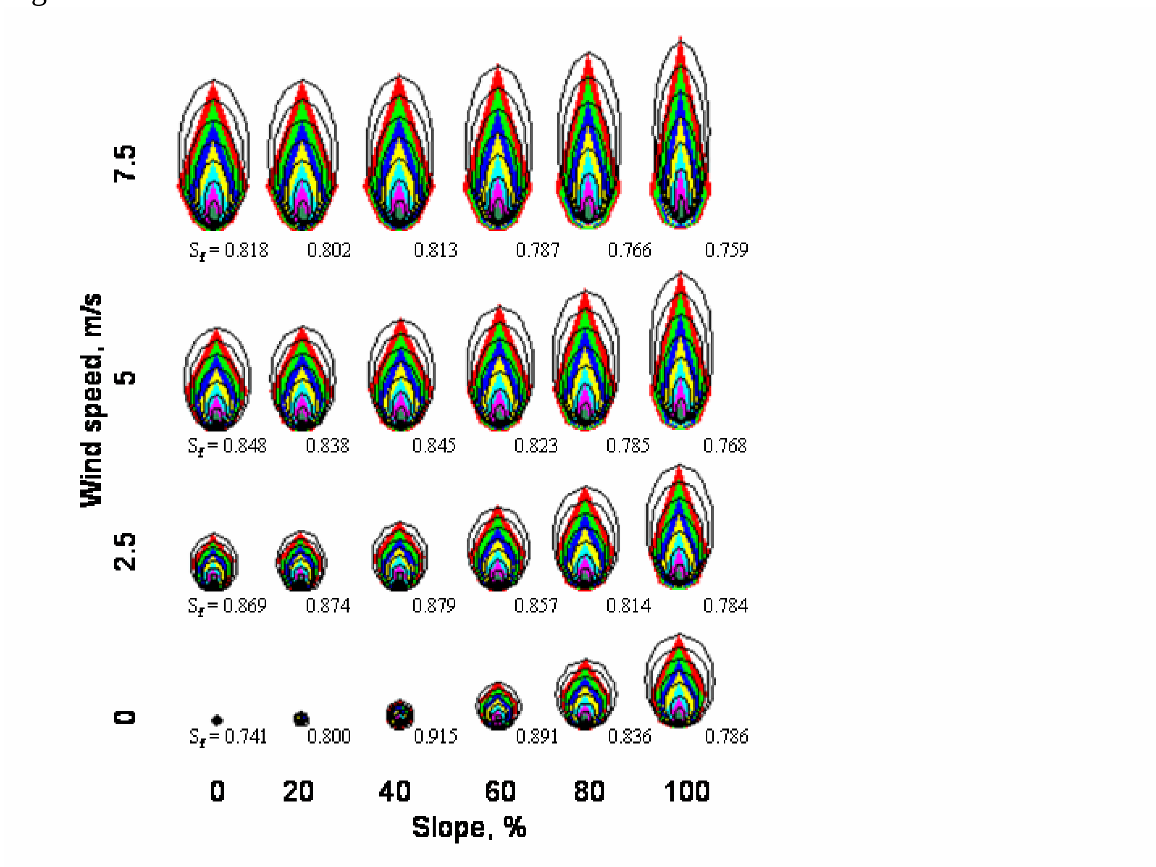
7.5
S_f = 0.818
0.802
0.813
0.787
0.766
0.759
Wind speed, m/s
5
S_f = 0.848
0.838
0.845
0.823
0.785
0.768
2.5
S_f = 0.869
0.874
0.879
0.857
0.814
0.784
0
S_f = 0.741
0.800
0.915
0.891
0.836
0.786
0
20
40
60
80
100
Slope, %

Figure 5

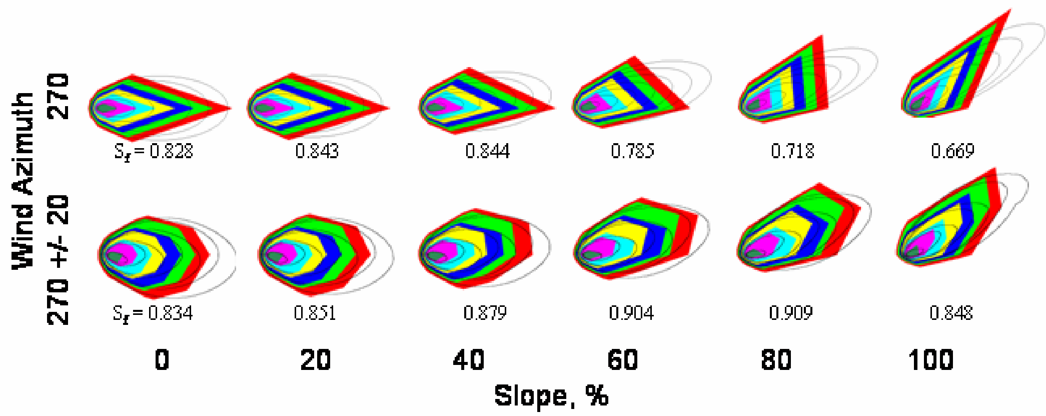

Wind Azimuth
270
270 +/- 20
S_f = 0.828
0.843
0.844
0.785
0.718
0.669
S_f = 0.834
0.851
0.879
0.904
0.909
0.848
0
20
40
60
80
100
Slope, %

Figure 6

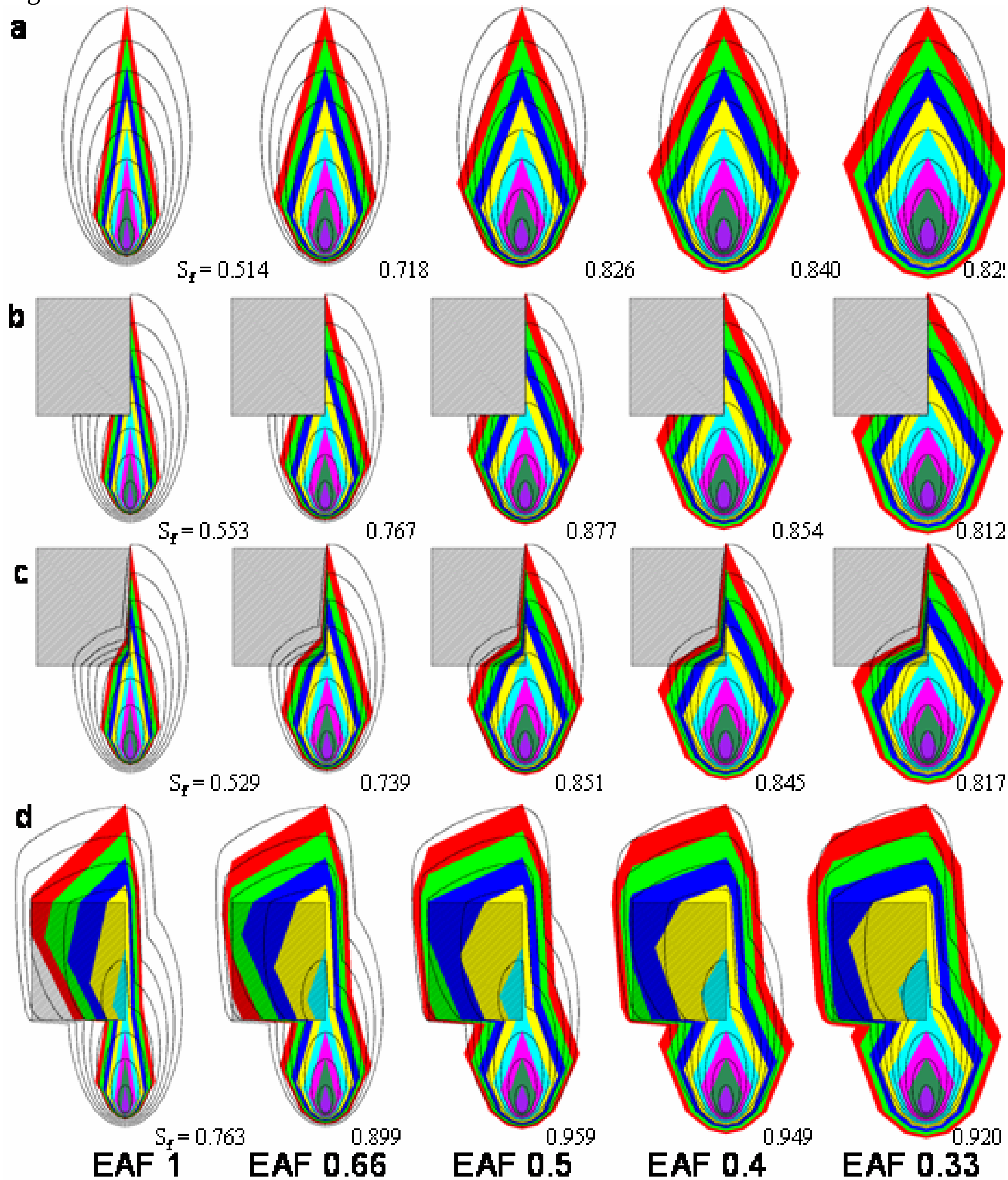

a
S_f = 0.514
0.718
0.826
0.840
0.82
b
S_f = 0.553
0.767
0.877
0.854
0.812
c
S_f = 0.529
0.739
0.851
0.845
0.817
d
S_f = 0.763
0.899
0.959
0.949
0.920
EAF 1
EAF 0.66
EAF 0.5
EAF 0.4
EAF 0.33

Figure 7

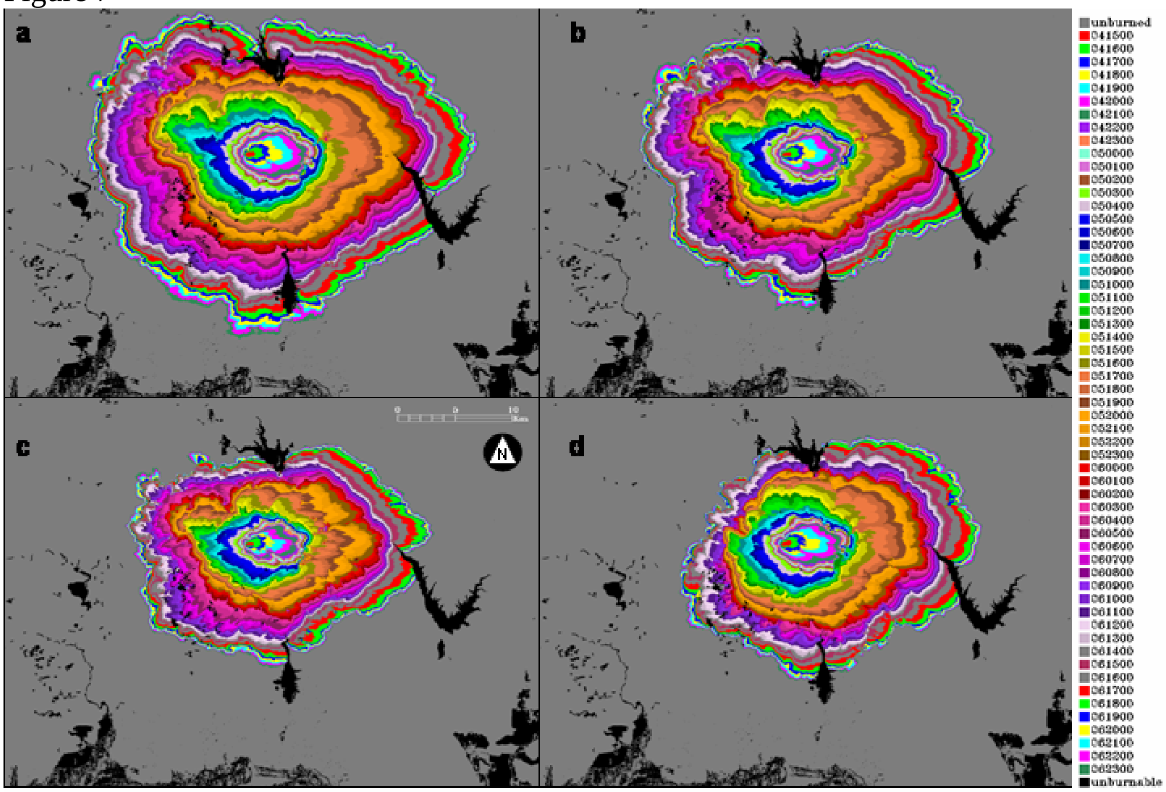

a
b
c
d
N
unburned
041500
041600
041700
041800
041900
042000
042100
042200
042300
050000
050100
050200
050300
050400
050500
050600
050700
050800
050900
051000
051100
051200
051300
051400
051500
051600
051700
051800
051900
052000
052100
052200
052300
060000
060100
060200
060300
060400
060500
060600
060700
060800
060900
061000
061100
061200
061300
061400
061500
061600
061700
061800
061900
062000
062100
062200
062300
unburnable

Figure 8

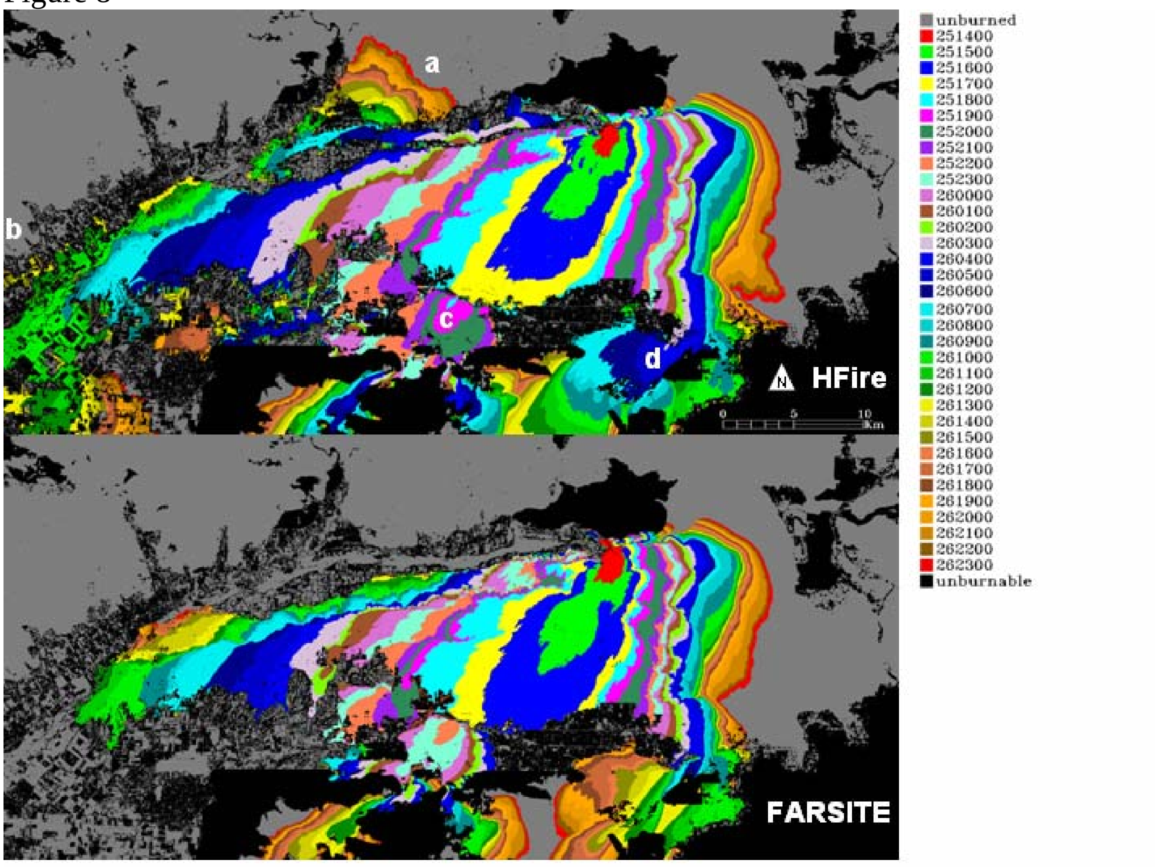
a
b
c
d
HFire
0 5 10 Km
FARSITE
unburned
251400
251500
251600
251700
251800
251900
252000
252100
252200
252300
260000
260100
260200
260300
260400
260500
260600
260700
260800
260900
261000
261100
261200
261300
261400
261500
261600
261700
261800
261900
262000
262100
262200
262300
unburnable

Figure 9

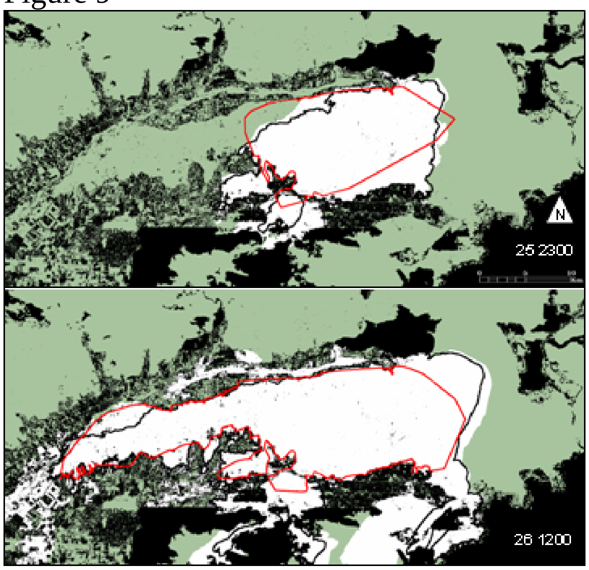

Time	Sørensen	Comparison
252300	0.762	MODIS/Hfire
252300	0.780	MODIS/Farsite
261200	0.445	MODIS/Hfire
261200	0.566	MODIS/Farsite

Figure 10

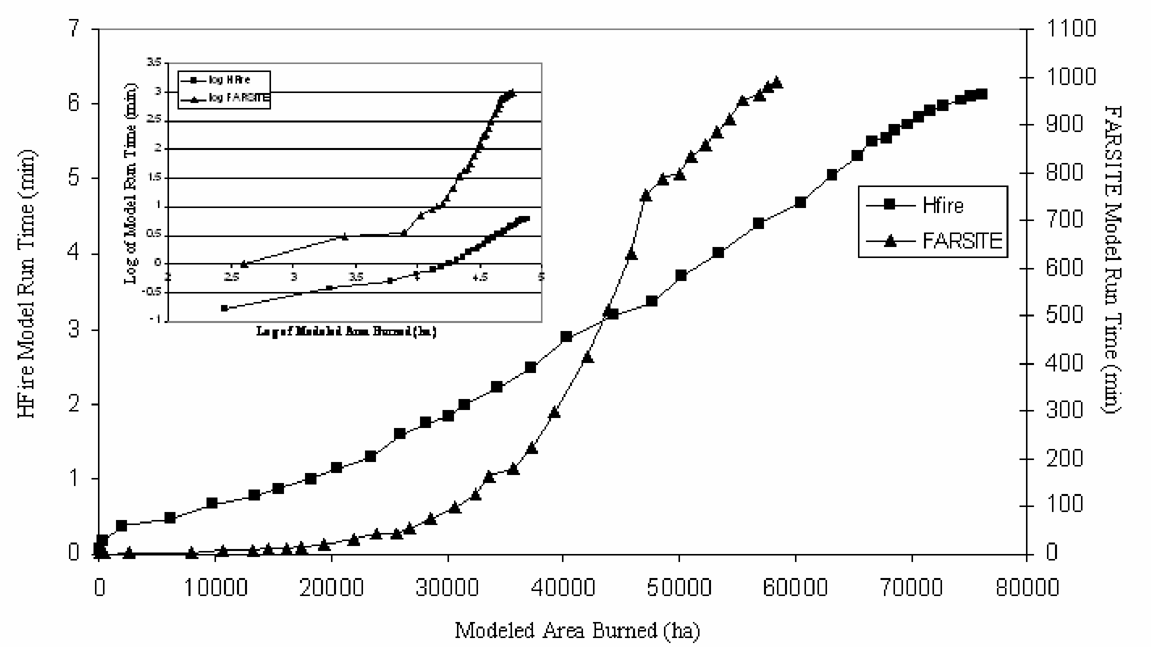

HFire Model Run Time (min)
FARSITE Model Run Time (min)
Modeled Area Burned (ha)
Hfire
FARSITE
Log of Model Run Time (min)
Log of Modeled Area Burned (ha)
log HFire
log FARSITE
0
1
2
3
4
5
6
7
0
100
200
300
400
500
600
700
800
900
1000
1100
0
10000
20000
30000
40000
50000
60000
70000
80000

Online Supplemental Material / Accessory Publication

5.2.3 Calabasas Fire

The 1996 Calabasas Fire burned 5159 hectares in the Santa Monica Mountains, California. The Calabasas Fire was chosen for simulation based on the availability of hourly perimeter data for the fire, and availability of remote sensing data for mapping pre-fire fuels. The Calabasas Fire was a Santa Ana wind driven event, typical of conditions under which the majority of burning takes place in shrublands of southern California (Keeley *et al.* 1999, Moritz *et al.* 2004). The fire was actively spreading from the time it started along U.S. Highway 101 on October 21, 1996 at approximately 1100 hours Pacific Daylight Time (PDT) until containment was achieved late on the morning of October 22. At one hour intervals during the course of the fire, a helicopter equipped with a Global Positioning Systems (GPS) receiver was used to map the location of the leading edge of the fire. These data serve as the historical record of fire spread to which the HFire and FARSITE simulations are referenced. The effects of suppression are unaccounted for in the simulations and therefore represent a potential source of error in comparing modeled and actual fire behavior. Suppression of the heading portion of the fire was largely unsuccessful during the first four hours of the fire, but suppression along the flanks of the fire during this time did have some effect (Herb Spitzer, Los Angeles County Fire Department, Pers. Comm.).

The northern and southern portions of the Calabasas Fire were modeled separately for comparison to the helicopter based reference perimeters. The northern portion of the fire occurred between 1100 and 1500 hours. A second simulation period, from 1500 to

2200 hours, was also examined as the spot fire over Malibu Canyon Road acted as a point source (Supplemental Figure 2).

#Insert Supplemental Figure 2 Approximately Here#

Historical wind speed, wind direction, and dead fuel moisture data during the fire are available on an hourly basis from the Cheesebro RAWS station, located 12 km from the fire. Live fuel moisture during the simulation was held constant at a value of 60% ODW for live herbaceous material and 60% ODW for live woody material.

Use of the most up to date map of fuels for the Santa Monica Mountains is inappropriate in a historical reconstruction because the current fuel type in the area of the 1996 Calabasas Fire reflects early post fire succession. Instead, a technique was devised to produce a fuels map to reflect the conditions in 1996, prior to the arrival of the fire. First, a map of the potential natural vegetation (PNV), the ultimate floristic composition an area would attain many years after fire, was generated using Franklin (1997). Second, the fire history of the Santa Monica Mountains was retabulated to reflect the age of each cell prior to the arrival of the Calabasas Fire. Finally, tables of successional pathways, referred to as regrowth files (.rgr), were used to cross reference each chaparral PNV type with age to yield a fuel type. The regrowth files included custom chaparral fuel models (Weise and Regelbrugge 1997), and were used to make maps showing custom fuels. Additionally, a custom fuel model for describing wildland-urban interface was developed by combining the fuel loadings in the NFFL grass and southern rough fuel models.

Terrain elevation for the entire domain is available at 10 meter spatial resolution. Since the spatial resolution of the fuels data is no better than 30 meters, the elevation data were resampled from 10 to 30 meters using bilinear interpolation prior to calculating slope and aspect at that resolution.

5.2.3.1 Calabasas Fire results

Supplemental Figure 3 shows the fire perimeters for HFire (EAF 0.66) and FARSITE for the single ignition case, with the fire igniting at 1100 hours and burning until 2200 hours. As for the Day Fire, agreement was highest for the 0.66 EAF case, and only EAF of 0.66 results are presented. The FARSITE simulation reaches the southern boundary approximately one hour sooner than HFire, but in general the shape and size of the fires are very similar. Sørensen metric values were on the order of 0.8 to 0.9. As for the Day Fire, these values compare favorably with the values for the synthetic landscape tests, suggesting that the complex landscapes serve to mitigate the raster/vector differences in predicted fire shape.

#Insert Supplemental Figure 3 Approximately Here#

However, comparing Supplemental Figures 2 and 3 reveals that agreement between the actual perimeters (Supplemental Figure 2) and perimeters from both models (Supplemental Figure 3) is poor. This is likely due to effective fire suppression efforts. The actual fire was much narrower during the initial 1100 to 1500 hours burning period, and was nearly controlled, before it spotted over Malibu Canyon road, igniting the second stage of the fire. Because of the compounding errors due to not accounting for fire suppression, HFire and FARSITE were rerun, treating the northern and southern halves of the fire separately.

Supplemental Figure 4 shows HFire, FARSITE, and actual perimeters at two times following the initial ignition at 1100 hours and two times following the spot fire ignition at 1500 hours. At 1300 and 1500 hours, both the azimuth and size of the modeled and actual fires differ. The Cheeseboro RAWS station is located 6 km northwest of the initial ignition point of the fire. Wind data from the Malibu RAWS station, which is located 10 km south southeast of the initial ignition point, were also examined but contained periods of winds blowing from the south so predictions showed less agreement with the historical perimeters. The Santa Monica Mountains have complex topography, so it is plausible that the winds are subject to topographic steering, and only a RAWS station within the same canyon as a fire would provide accurate wind azimuth data. An alternate explanation is that as RAWS "hourly" wind data are not actually hourly averages, but rather the average of the wind conditions five minutes prior to the reading, the data could be biased. The over prediction of fire size relative to the actual fire perimeter is again likely due to suppression.

#Insert Supplemental Figure 4 Approximately Here#

In contrast, modeled fire perimeters at the two later times, associated with the spot fire ignition, exhibit better agreement with the actual fire in both direction and magnitude of fire spread. Both the actual and modeled fires reached the southern end of the landscape (the Pacific Ocean) within the same hour. The modeled fires are narrower than the actual fire at 1800 hours but are on the same order of magnitude at 2200 hours. Sørensen metric values between HFire and the actual fire are also much higher at 1800 and 2200 hours than at 1300 and 1500 hours, on the order of 0.7 vs. 0.2.

Simulations of the Calabasas Fire demonstrate that HFire and FARSITE produce similar fire perimeters, and that correspondence between modeled and actual fire perimeters is very sensitive to input wind data, specifically wind direction in this case. In fact, manually adjusting the wind azimuth file for the first few hours to a more northerly direction results in excellent agreement between modeled and historical perimeters (not shown).

References

Franklin J (1997) Forest Service Southern California Mapping Project: Santa Monica Mountains National Recreation Area, Final Report. Unpublished report. 11p.

Keeley JE, Fotheringham CJ, Morais M (1999) Reexamining fire suppression impacts on brushland fire regimes. *Science* **284**, 1829-1832.

Moritz MA, Keeley JE, Johnson EA, Schaffner AA (2004) Testing a basic assumption of shrubland fire management: how important is fuel age? *Frontiers in Ecology and the Environment* **2**, 67-72.

Figure 1. Day Fire perimeters at 2300 hours on 6 September, Hfire (white), FARSITE (black), MODIS (red). The discrepancy in fire size between the modeled fires and the actual fire is attributable to fire suppression.

Figure 2. Fire Perimeters for the Calabasas Fire determined by helicopter reconnaissance. The pinched shape at 1500 hours is due to successful fire suppression efforts, which were nearly successful until the fire spotted over containment lines between 1500 and 1600 hours. Times are in MonthMonth/DD HHMM format.

Figure 3. Simulated perimeters for the Calabasas Fire for (a) HFire (EAF 0.66) and (b) FARSITE. Times are in DDHHMM format. Sørensen metric scores are included. Agreement is high throughout the simulation period.

Figure 4. Calabasas Fire perimeters, HFire (white), FARSITE (black), and helicopter reference (red), for the initial ignition and the spot fire ignition. The 1300 and 1500 hour perimeters result from the initial ignition at 1200 hours, the 1800 and 2200 hour perimeters result from the spot fire ignition at 1500 hours. Times are in DDHHMM format. Sørensen metric scores are included. The first set of simulations show poor agreement with reality because the wind azimuth recorded at the Cheeseboro RAWS was

not representative of the winds affecting the fire. Agreement was better during the second simulation period.

Figure 1

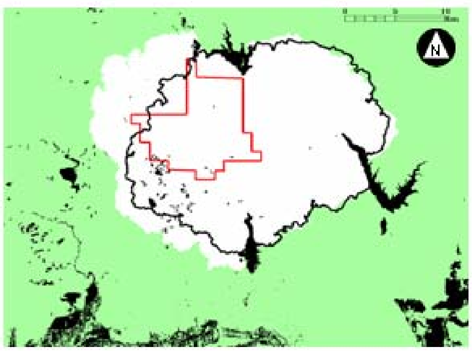

Figure 2

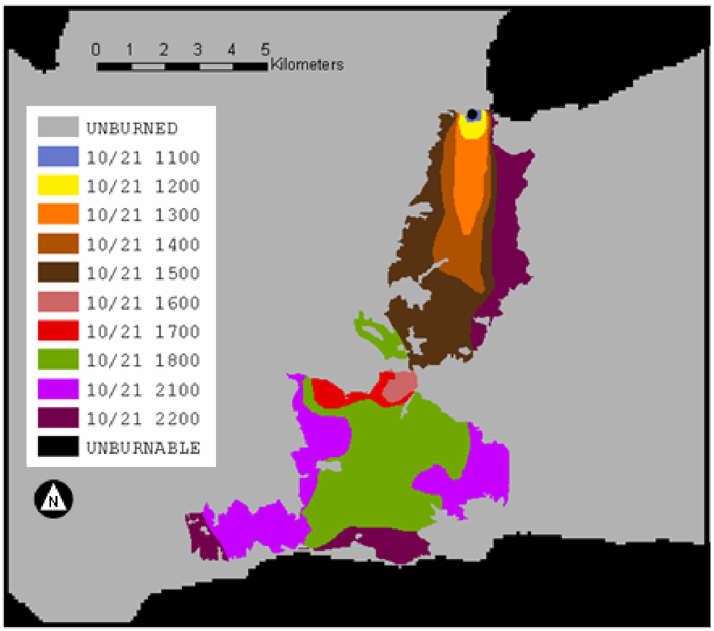
0 1 2 3 4 5
Kilometers
UNBURNED
10/21 1100
10/21 1200
10/21 1300
10/21 1400
10/21 1500
10/21 1600
10/21 1700
10/21 1800
10/21 2100
10/21 2200
UNBURNABLE
N

Figure 3

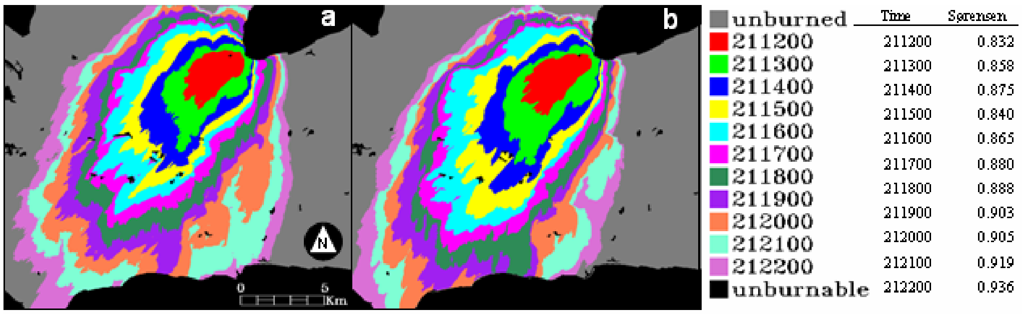
a
b
N
0 5 Km
unburned
211200
211300
211400
211500
211600
211700
211800
211900
212000
212100
212200
unburnable
Time Sørensen
211200 0.832
211300 0.858
211400 0.875
211500 0.840
211600 0.865
211700 0.880
211800 0.888
211900 0.903
212000 0.905
212100 0.919
212200 0.936

Figure 4

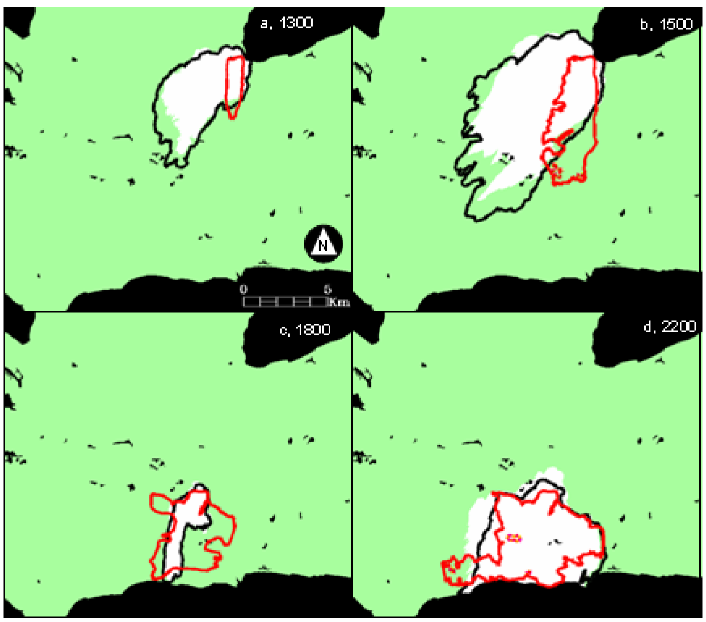

	Sørensen	
Time	Hfire	FARSITE
211200	0.140	0.121
211300	0.211	0.199
211400	0.229	0.227
211500	0.298	0.282

	Sørensen	
Time	Hfire	FARSITE
211600	0.505	0.597
211700	0.513	0.524
211800	0.548	0.529
211900	0.764	0.742
212000	0.709	0.758
212100	0.750	0.799
212200	0.742	0.810

Table 1. Sørensen metric values for HFire (EAF set to 0.5, 0.66, and 0.9) and FARSITE for the Day Fire, with. The EAF 0.66 model run shows the highest agreement with FARSITE, with Sørensen values on the order of 0.9.

EAF 0.5				EAF 0.66				EAF 0.9			
Time	Sørensen	Time	Sørensen	Time	Sørensen	Time	Sørensen	Time	Sørensen	Time	Sørensen
41500	0.819	51900	0.835	41500	0.774	51900	0.904	41500	0.632	51900	0.772
41600	0.922	52000	0.829	41600	0.919	52000	0.911	41600	0.827	52000	0.787
41700	0.898	52100	0.824	41700	0.899	52100	0.913	41700	0.792	52100	0.8
41800	0.875	52200	0.821	41800	0.877	52200	0.913	41800	0.725	52200	0.807
41900	0.889	52300	0.819	41900	0.907	52300	0.914	41900	0.729	52300	0.817
42000	0.902	60000	0.814	42000	0.915	60000	0.911	42000	0.732	60000	0.823
42100	0.918	60100	0.806	42100	0.94	60100	0.906	42100	0.777	60100	0.832
42200	0.92	60200	0.798	42200	0.959	60200	0.902	42200	0.813	60200	0.841
42300	0.914	60300	0.784	42300	0.965	60300	0.893	42300	0.833	60300	0.849
50000	0.905	60400	0.765	50000	0.966	60400	0.881	50000	0.853	60400	0.856
50100	0.898	60500	0.745	50100	0.962	60500	0.862	50100	0.861	60500	0.858
50200	0.89	60600	0.73	50200	0.96	60600	0.847	50200	0.859	60600	0.855
50300	0.878	60700	0.72	50300	0.962	60700	0.838	50300	0.853	60700	0.851
50400	0.876	60800	0.72	50400	0.958	60800	0.838	50400	0.849	60800	0.85
50500	0.876	60900	0.723	50500	0.959	60900	0.839	50500	0.859	60900	0.848
50600	0.864	61000	0.728	50600	0.957	61000	0.841	50600	0.869	61000	0.847
50700	0.857	61100	0.737	50700	0.957	61100	0.846	50700	0.868	61100	0.847
50800	0.855	61200	0.746	50800	0.96	61200	0.853	50800	0.865	61200	0.853
50900	0.847	61300	0.75	50900	0.949	61300	0.855	50900	0.859	61300	0.854
51000	0.838	61400	0.754	51000	0.937	61400	0.859	51000	0.855	61400	0.854
51100	0.835	61500	0.761	51100	0.925	61500	0.864	51100	0.832	61500	0.854
51200	0.839	61600	0.76	51200	0.911	61600	0.869	51200	0.809	61600	0.861
51300	0.846	61700	0.757	51300	0.904	61700	0.872	51300	0.789	61700	0.867
51400	0.85	61800	0.753	51400	0.898	61800	0.873	51400	0.779	61800	0.872
51500	0.845	61900	0.751	51500	0.899	61900	0.872	51500	0.779	61900	0.874
51600	0.843	62000	0.748	51600	0.894	62000	0.871	51600	0.776	62000	0.874
51700	0.839	62100	0.745	51700	0.89	62100	0.87	51700	0.767	62100	0.875
51800	0.84	62200	0.742	51800	0.892	62200	0.869	51800	0.763	62200	0.875
		62300	0.739			62300	0.868			62300	0.875

Table 2. Sørensen metric values for HFire (EAF set to 0.66) and FARSITE for the Simi Fire. Accuracy is lower at the beginning and end of the model runs. At the beginning FARSITE is propagating the fire more quickly, at the end the HFIRE modeled fire is larger as it is better able to negotiate narrow fuel isthmuses.

Time	Sørensen	Time	Sørensen
251400	0.714	260700	0.854
251500	0.769	260800	0.852
251600	0.827	260900	0.845
251700	0.926	261000	0.847
251800	0.944	261100	0.84
251900	0.924	261200	0.838
252000	0.905	261300	0.837
252100	0.898	261400	0.842
252200	0.901	261500	0.846
252300	0.915	261600	0.851
260000	0.915	261700	0.856
260100	0.915	261800	0.859
260200	0.917	261900	0.862
260300	0.904	262000	0.864
260400	0.899	262100	0.865
260500	0.888	262200	0.865
260600	0.86	262300	0.866